Relative sea-level data from southwest Scotland constrain meltwater-driven sea-level jumps prior to the 8.2 kyr BP event

Thomas Lawrence*[1], Antony J. Long[1], W. Roland Gehrels[2], Luke Jackson[3], David E. Smith[4]

[1]Dept. of Geography, Lower Mountjoy, Durham University, South Road, Durham, DH1 3LE
[2]Environment Dept., York University, Heslington, York, YO10 5NG
[3]New Institute for Economic Thinking, Eagle House, Oxford University, OX2 6ED
[4]Geography and Environment Dept., St Edmund Hall, Oxford University, OX1 4AR

*corresponding author (thomas.lawrence@durham.ac.uk)
Keywords: sea level, 8.2 ka event, early Holocene, ice-sheet, lake drainage, Scotland

Abstract

The most significant climate cooling of the Holocene is centred on 8.2 kyr BP (the '8.2 event'). Its cause is widely attributed to an abrupt slowdown of the Atlantic Meridional Overturning Circulation (AMOC) associated with the sudden drainage of Laurentide proglacial Lakes Agassiz and Ojibway, but model simulations have difficulty reproducing the event with a single-pulse scenario of freshwater input. Several lines of evidence point to multiple episodes of freshwater release from the decaying Laurentide Ice Sheet (LIS) between ~8900 and ~8200 cal yr BP, yet the precise number, timing and magnitude of these events – critical constraints for AMOC simulations – are far from resolved. Here we present a high-resolution relative sea level (RSL) record for the period 8800 to 7800 cal yr BP developed from estuarine and salt-marsh deposits in SW Scotland. We find that RSL rose abruptly in three steps by 0.35 m, 0.7 m and 0.4 m (μ) at 8760-8640, 8595-8465, 8218-8323 cal yr BP respectively. The timing of these RSL steps correlate closely with a variety of short-lived events expressed in North Atlantic proxy climate and oceanographic records, providing evidence of at least three distinct episodes of enhanced meltwater discharge from the decaying LIS prior to the 8.2 event. Our observations can be used to test the fidelity of both climate and ice-sheet models in simulating abrupt change during the early Holocene.

1. Introduction

A prominent climate anomaly is centred on 8200 yr BP in Greenland ice-core records (Figs. 1 and 2) and is registered as an abrupt cooling of ~3.3 ± 1.1 °C that lasted for 160 yrs (Kobashi et al., 2007; Thomas et al., 2007). The widely cited (e.g. Alley et al., 1997; De Vernal et al., 1997; Barber et al., 1999; Törnqvist and Hijma, 2012) causal mechanism of the event is a weakening or complete shutdown of the Atlantic Meridional Overturning Circulation (AMOC) in response to the sudden drainage of Laurentide proglacial Lakes Agassiz and Ojibway (LAO) dated to 8740-8160 cal yr BP (1σ age range) in the Hudson region (Barber et al., 1999). However, it is unclear whether the drainage occurred as a standalone freshwater pulse or as several separate events. Indeed, climate modelling studies based on a single freshwater pulse of 2.5 Sv for one year (Sverdrup, 1.0 = 10^6 m^3 s^{-1}) fail to simulate the observed 8.2 climatic response (Morrill et al., 2014) using a median estimate of forcing inferred from flood hydrograph simulations of the final LAO drainage (Clarke et al., 2004).

A growing body of empirical and modelling evidence is beginning to support a multi-event model of LAO drainage (Leverington et al., 2002) and/or nonlinear Laurentide Ice Sheet (LIS) collapse within a critical time interval (hereby referred to as 8900 to 8200 cal yr BP). Pronounced two-step increases in planktonic $\delta^{18}O$ and polar foraminifera abundance (*Neogloboquadrina pachyderma* s.) occur in two sub-polar North Atlantic cores, MD99-2251 and MD03-2665, situated 1250 km apart, that are interpreted as two episodes of increased surface ocean freshening and cooling within this time interval (Fig. 2; Ellison et al., 2006; Kleiven et al., 2008). Hematite-rich glaciolacustrine sediments in the Hudson region (the "red-bed") widely thought to represent the stratigraphic signature of LAO drainage (e.g. Barber et al., 1999; Hillaire-Marcel et al., 2007), contain two peaks of terrestrially-sourced detrital carbonate (Hillaire-Marcel et al., 2007) and two stacked sequences of reverse to normal graded sediments which could record two separate drainage events (Lajeunesse and St-Onge, 2008).

Recent evidence from shelf-sea and estuarine sediments complicate the story as these contain evidence of a third event. A well-resolved near-field record of LIS retreat is provided by Jennings et al. (2015), who observed detrital carbonate peaks (DCPs) at 8694-8609 (DCP6a), 8609-8489 (DCP6b) and 8219-7998 cal yr BP (DCP7) (Fig. 2g) in Cartwright Saddle core MD99-2236, which they attribute to episodes of abrupt freshwater discharge. The second event, DCP6b, is manifest as the downstream equivalent of the Hudson Bay "red-

bed", which Jennings et al. (2015) re-interpret as a final phase in the abrupt opening of the Tyrrell Sea following retreat of Laurentide ice – not a drainage of LAO. Recent ice-sheet modelling predicts that the dynamic separation, or "saddle-collapse" of the Keewatin and Labrador domes, which occurred during deglaciation over the Tyrrell Sea, produced a meltwater pulse with peak discharge rates of ~0.21 Sv between ~8800 and ~8600 yrs BP (Gregoire et al., 2012). This provides a possible mechanism for a meltwater pulse concomitant with the Tyrrell Sea 'opening' event. Jennings et al. (2015) interpret the later event, DCP7, as the signature of LAO drainage(s) due to its close coincidence with the 8.2 event. However the significance of DCP7 in forcing the 8.2 event is unclear as it post-dates the onset of the 8.2 event, dated at ~8247 cal yr BP (Thomas et al., 2007), by a minimum c. 30 yrs, albeit this could reflect chronological uncertainties within the Jennings et al. (2015) record (i.e., the 8.2 to 9.7 ka BP time interval is constrained in this record by two ^{14}C ages). Nevertheless, this three-event model of abrupt freshwater discharge is supported by estuarine records from the Gulf of Mexico where Simkins et al. (2012) observed prominent magnetic susceptibility anomalies at ~8800, ~8600 and ~8100 cal yr BP. It is suggested that previous near-field sea-bed records that describe evidence of one or two events (Hillaire-Marcel et al., 2007; Hoffman et al., 2012) are limited by core resolution and may record additional events (Jennings et al., 2015).

Notwithstanding the limited chronological control across the critical time interval, the Cartwright Saddle record from core MD99-2236 arguably provides the best-resolved near-field history of final LIS retreat because of its relatively high resolution and stratigraphic continuity. The interpretation of a three-event freshwater discharge model includes the potential abrupt drainage(s) of LAO as well as a possible large ice-sheet contribution associated with the saddle collapse of the Keewatin and Labrador domes (Gregoire et al., 2012). If correct, the causal mechanisms of the 8.2 event are more complex than that suggested by the consensus view of a single- or double-event drainage of LAO. The Jennings et al. (2015) record describes a sequence of freshwater events prior to the 8.2 event but little is known regarding the magnitudes of such events, critical constraints for modelling studies of the AMOC. Understanding the pathways of freshwater routing is also critical as some authors predict transport into the sub-tropical North Atlantic (Condron and Windsor, 2011; Hill and Condron, 2014) rather than the sub-polar gyre (Jennings et al., 2015; Kleiven et al., 2008; Ellison et al., 2006).

Relative sea-level (RSL) records provide a means to test the hypothesis that the DCP events in Cartwright Saddle core MD99-2236 were significant freshwater discharge events from the LIS. Regional land-based water/ice mass variability will alter the geoid thus producing an associated sea-level pattern, also termed "fingerprint", that is non-uniform across the globe (e.g. Mitrovica et al., 2001). In the case of a point source of land water/ice mass loss, RSL will be negative near to the former source location and positive in the intermediate to far-field regions. This is illustrated in Fig. 1, which shows the predicted percentage of the global sea-level equivalent mass loss from the drainage of Lake Agassiz-Ojibwa at 8.4ka (Kendall et al., 2008) using a geophysical model to solve the sea-level equation (Mitrovica & Milne, 2003).

Three well-dated RSL records based on radiocarbon-dated basal peats (therefore minimally affected by sediment compaction) exist for the centuries prior 8.2 ka, and both contain an abrupt departure from background rates of RSL rise, or a RSL 'jump'. In the western Netherlands (Rhine-Meuse Delta), Hijma and Cohen (2010) define a eustatic equivalent sea-level jump of 3.0 ± 1.5 m at 8590-8350 cal yr BP, while in the Mississippi Delta, Li et al. (2012) identify a eustatic jump of 1.2 ± 0.2 m at 8310-8180 cal yr BP. Both jumps are corrected for a Laurentide source of mass loss using geophysical modelling predictions (Kendall et al., 2008). It has been suggested that due to differences in the timing and magnitude of the two RSL jumps, the Rhine-Meuse jump contains two separate events, while the Mississippi Delta record captures a final event only (Törnqvist and Hijma, 2012; Li et al., 2012). Indeed, the Mississippi Delta record contains a reworked pre-event stratigraphy dated to ~8400 cal yr BP which has been interpreted as possible evidence of a preceding RSL jump (Li et al., 2012). The third well-dated RSL record is from the Ythan estuary, Scotland, and discloses a RSL jump of between 2.56m and 4.77m, dated at between 8177-8366 cal yr BP and 8445-8637 cal yr BP (2σ ranges), but no evidence for more than one jump is quoted (Smith et al., 2013).

The Rhine-Meuse, Mississippi Delta and Ythan estuary records lack conclusive bio- and lithostratigraphic evidence of more than one event found in continuous stratigraphic sequence. Therefore, at present the sea-level data are unable to test the hypothesised three-stage LIS retreat model of Jennings et al. (2015).

Here we present a stratigraphically continuous record of RSL for Blair's Croft in the Cree Estuary, SW Scotland, which is sub-centennially resolved for the period ~8800 to ~7800 cal yr BP. In particular, we test two hypotheses: (1) that RSL rose abruptly in more than one

abrupt step in the several centuries prior to 8.2 event, and (2) that the RSL jump(s) correlate with other short-lived event(s) observed in various North Atlantic proxy records.

2. Field site

The Cree Estuary is situated on the northern shores of the Solway Firth (N 54°51', W 4°30'). The River Cree is tidal from Newton Stewart and drains southwards through the Cree coastal lowlands into Wigtown Bay (Fig. 3B). The predicted present day spring tidal range in Wigtown Bay is 6.40 m (supplementary info Fig. S1; Ward, 2014), which is comparable to the range of 6.70 m obtained from the tide gauge in the adjacent small (up-) estuary harbour of Kirkudbright (Fig. 3B; Admiralty Tide Tables, 2014). The Cree coastal lowlands (i.e., the area below the 10 m OD (OD = UK geodetic datum; where 0 m OD = approximate mean tide level) contour line; Fig. 3C) have been the focus of several previous RSL studies (e.g. Jardine, 1975; Bishop and Coope, 1977; Smith et al., 2003a). In the most recent of these, Smith et al. (2003a) reported that RSL rose from -6 m OD at ~9500 to a mid-Holocene RSL highstand of +6 m OD at ~5500 cal yr BP before falling to present. One of the sites used to constrain this RSL history is Blair's Croft, located ~1.5 km inland of the current tidal limit and at the base of the Galloway National Park foothills, where a sequence of interbedded estuarine and salt-marsh deposits are preserved below a surface freshwater peat. These deposits were dated by Smith et al. (2003a) using conventional bulk radiocarbon dating to within the broad timeframe of the 8.2 event, although not fully attributed to the event itself. These sediments provide the basis for this study.

3. Methods

3.1 Lithostratigraphy

We conducted further lithostratigraphic investigations at Blair's Croft, paying particular attention to the sediments that were originally dated by Smith et al. (2003a) as spanning the centuries either side of the 8.2 event, i.e. between ~8800 and 7800 cal yr BP (Figs. 4 and 5). Fifty hand-cores were sunk along three transects. Sediments were classified with reference to

the Troels-Smith (1955) scheme of stratigraphic notation. Each transect commenced at the break of slope at the valley-side and extended westward by 100-200 m towards the A75 trunk road and the present-day estuary. No further cores were sunk on the western side of the A75 road in Carsewolloch Flow, as Smith et al. (2003a) and Wells (1997) here reported a broadly homogenous sequence of estuarine clays (i.e., no inter-bedded organic deposits). Sample core BC421 (Transect 1) was deemed representative of wider changes at Blair's Croft and was collected using a modified piston corer with 0.7-1.0 m overlapping lengths. Some compaction was observed during sampling and corrected for based on the depths recorded in an adjacent hand core. We account for this correction with a conservative 0.2 m uncertainty (Section 3.4).

3.2 Laboratory methods

We conducted microfossil (diatom) analyses in order to determine estimates of past sea level. Samples were prepared using standard techniques (Palmer and Abbott, 1986), identified with reference to the taxonomy of Hartley et al. (1996) and grouped according to a simplified halobian classification scheme of Vos and de Wolf (1993). A total of 74 samples were taken at ~4 cm intervals. We counted a minimum of 200 valves, with the exception of 10 samples that contained a count of 150-200 valves. Percentage loss-on-ignition was measured on 4 g subsamples to identify horizons with relatively high organic content (>20%) indicative of upper intertidal and supratidal conditions. Samples were weighed prior to being oven-dried overnight at 80°C, reweighed, combusted at 550°C for four hours and weighed again.

Our chronology is constrained by 13 Accelerator Mass Spectrometry (AMS) ^{14}C determinations of individual terrestrial plant macrofossils (Table 1). Ages are reported as 2σ ranges, calibrated (IntCal13; Reimer et al., 2013) with respect to BP (where BP = AD 1950). Our dating was performed at the Scottish Universities Environmental Research Centre, NERC radiocarbon facility in East Kilbride, UK, on cleaned, horizontally-bedded plant macrofossils (*Phragmites australis*) and c. 1cm^3 wood (*Alnus*) fragments that were intact and away from the core edges. All ^{14}C samples were pre-treated using standard methods (e.g. Czernik and Goslar, 2001) in East Kilbride. Most samples were dated twice and subject to a weighted mean using the "R_combine" function of OxCal 4.2 (Bronk Ramsey, 2008) in an attempt to increase the precision of uncalibrated ^{14}C ages (i.e. the reported 1σ laboratory errors, Marshall et al., 2007; Li et al., 2012). Ages were modelled with an OxCal 4.2 "P_Sequence" function, which takes into account stratigraphic information and thus assumes

that calibrated ages increase with depth, i.e., that no age reversals are allowed. Such models have shown to improve accuracy and retain precision (e.g. Bronk Ramsey, 2000).

3.3 Transfer function development

To reconstruct RSL from fossil diatom assemblages, we exploit the relationship between the distribution of their modern counterparts with marsh surface elevation (e.g. Zong and Horton, 1999; Barlow et al., 2013), which is primarily controlled by the frequency of tidal flooding (hence, RSL). The elevation of an assemblage relative to tide levels is termed its 'indicative meaning'. Underpinning this is the assumption that the indicative meanings of contemporary diatoms and their assemblages remain unchanged through time. We apply the Barlow et al. (2013) transfer function to our fossil assemblages using the computer software C^2 v.1.6 (Juggins, 2011). The Barlow et al. (2013) dataset, although based on nine separate modern records from western Scotland, is lacking a key taxon that forms a large component of the Blair's Croft fossil record, *Tryblionella navicularis,* and which is essential to our reconstruction. Within present-day UK salt-marshes this taxon has only been documented in suitable abundances in Brancaster Marsh, Norfolk, eastern England, where it is found around the level of MHWST within an area characterised by *Phragmites australis* (supplementary info Fig. S2; Gehrels et al., 2001). In view of the abundance of *P. australis* macrofossil remains in the Blair's Croft organic beds, these appear to be analogous environments. All taxa from the Brancaster samples are included in addition to *T. navicularis*, which are integrated by standardizing their elevations (with respect to tidal range) with the standard water level index (SWLI) equation (Barlow et al., 2013):

$$SWLI_n = 100(h_n - h_{MTL}) / (h_{MHWST} - h_{MTL}) + 100 \quad (1)$$

where $SWLI_n$ is the standard water level index for a given sample *n*, h_n is the elevation of a given sample *n* (in metres OD), h_{MHWST} is the local mean height of spring tide and h_{MTL} is the local height of mean tide level. A SWLI of 100 and 200 are equivalent to MTL and MHWST, respectively.

Transfer function-based estimates of palaeo-RSL are calculated with respect to the modern tidal regime so they require correction for palaeotidal change. Estimates of the elevation of the height of MHWST for Wigtown Bay are provided by the palaeotidal model of Ward (2014), which indicates a reduction in MHWST height (based on $M_2 + S_2$ tidal components) from 3.27 m OD at 9.0 ka BP to 3.00 m OD at 8.0 ka BP (supplementary info Fig. S1). As most of our record encompasses this 1 kyr interval, we correct our data points using simple linear interpolation of the points between the 9.0 and 8.0 ka BP time-slices (supplementary info Fig. S1). We assume a fixed height of MTL (=0 m OD) across the time interval, such that the only fluctuating variable is MHWST height. The resulting correction applied is specific to each data point and uses the corresponding age inferred from the age model. No attempt was made to correct the few samples younger than 8.0 ka BP with a second linear function for the 8.0 to 7.0 ka BP time period; instead we extrapolate the same linear function. Uncertainties in the Ward (2014) model are yet to be rigorously quantified (Ward, pers. comm), so we introduce an arbitrary measure of uncertainty of 0.20 m for each data point. This is significantly larger than 2 standard error of the mean of the palaeotidal data (0.06 m) (Section 3.4). Transformation of the SWLI values back to OD is achieved using:

$$OD_n = (SWLI_n - 100) \times (PTH_{MHWST} - PTH_{MTL}) / 100 \quad (2)$$

where OD_n is the height of a given sample relative to ordnance datum, $SWLI_n$ is the standard water level index of a given sample, PTH_{MHWST} is the local height of mean high water of spring (palaeo)tide for the appropriate time period of interest (inferred from the age model) and PTH_{MTL} is the local height of mean (palaeo) tide level for the appropriate time period of interest (assumed zero).

3.4 Sea-level reconstruction

The combined uncertainty of each RSL data point comprises three error components (supplementary info Table S1); a) bootstrapped 1 SEM values of indicative meanings predicted by the modified Barlow et al. (2013) transfer function that includes *T. navicularis* (average +0.56 m; 1σ) and, b) the uncertainty of the palaeotidal correction (0.20 m). Thirdly,

we have linearly corrected for the difference between logged depths in a hand core and extruded depths from a piston core, for which we conservatively introduce a further 0.20 m to account for. All of the above terms are expressed as bidirectional 1σ uncertainties. We propagate these individual terms in a mean squared estimate to produce a combined uncertainty for each data-point:

$$\text{Mean squared estimate} = \sqrt{(a^2 + b^2 + c^2)} \quad (3)$$

The indicative meanings for each data point are converted to RSL using: $S = H - I$, where S is the height of relative sea-level (m OD), H is the height of the given sample (m OD) and I is the indicative meaning of the fossil sample (m OD).

To perform the sea-level reconstruction, we adapt the method of Rohling et al. (2014) by altering our method of random sampling in time and space. The conservative approach to constructing random samples from a set of RSL indicators is to randomly sample each in time independently and space independently. This approach assumes the RSL indicators are independent in terms of their relationship to each other. Problematically an individual RSL realisation (one sample drawn from each indicator), from the independently sampled data set may have reversals in time and space due to the overlapping uncertainties of adjacent indicators. In the case where data is derived from a single core, with stratigraphic order to the indicators, the conservative sampling method is physically implausible. To account for this dependency, yet allow for each RSL indicator to remain randomly sampled, we use the following strategy. We randomly sample the first and second RSL indicators. For each sample of the first RSL indicator we identify which quantile it falls within in time and space. We then tie it to a sample from the second RSL indicator drawn from those lying in the same time/space quantiles as the first. The next RSL indicator is then randomly sampled and each sample in the previous indicator tied to one in the newly sampled indicator. By applying this method to the set of RSL indicators we retain their order whilst sampling each randomly. We produce 1000 realisations of the RSL indicators, sampling each RSL indicator 1000 times. This novel approach to sampling is an attempt to reduce the uncertainties of the reconstruction given the wide uncertainties in time and space of the RSL indicators relative to the decimetre and decadal-to-centennial scale of DCP events that we seek to identify.

The remaining part of the reconstruction method follows Rohling et al. (2014), where we linearly interpolate each of the 1000 realisations to create time series with 10 year step size. We then calculate mean and standard deviations of the interpolated realisations at each

time step. We also remove spurious fluctuations by smoothing the reconstructed curves with a 50 year moving window. This degree of smoothing is minimal and does not significantly influence the results.

To determine rates of RSL, we employ two methods. The first is a sea-level rate reconstruction that uses the same method as outlined above, but differentiates a smoothed version of each linearly interpolated realisation. Following this, we calculate mean and standard deviations of the derived rates at each time step. The second approach is to differentiate the smoothed RSL reconstruction and its uncertainty bounds. While the first method is conservative in that it represents the full range of uncertainty in the rate derived from random sampling, the second assumes that the shape of RSL reconstruction is true, regardless of its vertical offset from the mean. For each method, the mean RSL rate reconstruction ($\mu_{dRSL/dt}$) and differentiated mean RSL reconstruction ($d\mu_{RSL}/dt$) give effectively the same result (see Results).

3.5 Developing comparative chronologies from ocean and ice core records

We test hypothesis (2); whether the timing of RSL jumps correlate with other abrupt events expressed in North Atlantic proxy records, by comparing the timing of sea-level accelerations/jumps within our record with those observed in various climate proxy records from the North Atlantic. Where resolution permits, we focus on comparing the start of events rather than event maxima within their respective chronologies.

3.5.1 Inferring the timing of abrupt North Atlantic events

We infer the onset of the two-step increases recorded in the surface $\delta^{18}O$ record from the North Atlantic (FE_1 and FE_2; Fig. 2h) (Kleiven et al., 2008) following new age modelling of the Kleiven et al. (2008) chronology, which was previously based on simple linear interpolation of ^{14}C ages. The Kleiven et al. (2008) observations are supported by a second planktonic foraminiferal dataset retrieved some 1250 km away in core MD99-2251 which also contains two abrupt anomalies (Figs. 2e and 2h) (Ellison et al., 2006), although the records are offset by c. 250 yrs, likely because of the limited age control of MD99-2251. For instance the chronology for MD99-2251 (Ellison et al., 2006) contains only two ages within

the critical time interval compared to the nine in MD03-2665 (Kleiven et al., 2008). As a result, we do not include the Ellison et al. (2006) record in our comparison, but nevertheless assume that the two-step anomalies in both records are expressions of the same events (Kleiven et al., 2008) and that the age offset reflects the limitations of the Ellison et al. (2006) chronology.

Of the nine dates between 9.0 to 8.0 kyr BP in the Kleiven et al. (2008) record, two are reversed. To correct this offset Kleiven et al. (2008) introduced a local reservoir value (ΔR) of 23 yrs to account for an enhanced East Greenland Current coincident with North Atlantic freshwater perturbation(s). We are unable to assess the reliability of this interpretation, but it is one we follow given the internal consistency of ΔR corrected ages. To ensure chronological robustness, we model the original Kleiven et al. (2008) ^{14}C data in OxCal 4.2 using a *P_sequence* function, after conservatively doubling (arbitrarily) the local ΔR uncertainties applied to the two ages with reversals. We then propagate the original laboratory 1σ errors of each ^{14}C age in a mean squared estimate. The modelled ages of MD03-2665 demonstrate strong internal agreement (96% overall model agreement index).

Next we infer the timing of the start of the two *N. pachyderma* δ^{18}O peaks from the adjusted chronology of Kleiven et al. (2008). However, we need to determine the precise onset of each anomaly within MD03-2665 with respect to core depth. The first abrupt increase in δ^{18}O occurs at 332 cm, while the initial drop in δ^{13}C in benthic foraminifera occurs at 346 cm in the same core (equivalent to ~70 yrs within the chronology). As this is likely indicative of a transfer delay between ocean surface and bottom waters in registering the freshwater anomaly (Kleiven et al. 2008), the earliest manifestation of the underlying anomaly, i.e.; the start of the δ^{13}C excursion, is therefore a more accurate representation of the start of the underlying freshwater event. This is supported by an increase in magnetic properties that is coeval with the onset of the δ^{13}C excursion. To infer the onset of the second anomaly, we have no choice but to use the δ^{18}O record because the δ^{13}C series records a broad minimum spanning several centuries rather than two distinct events.

From proximal to the former LIS margin we also include the timing of three DCPs observed in core MD99-2236 (Jennings et al., 2015). Improving the Jennings et al. (2015) chronology with Bayesian modelling is not necessary given that the critical interval of this record is constrained by only two ages. To tie in existing RSL observations from elsewhere, we compare age probability density functions of the onset of the Rhine-Meuse Delta RSL jump (Hijma and Cohen, 2010) and the full range of the Mississippi Delta RSL jump (Li et

al., 2012). Finally, although poorly constrained by dating, we also discuss the peak timing of the modelled Keewatin-Labrador ice-dome saddle collapse (Gregoire et al., 2012) and its possible significance within the sequence of observations. To provide insights into possible leads and lags, we calculate minimum and maximum age intervals between each event and the 8.2 event by subtracting the minimum and maximum estimates of their respective 2σ calibrated ranges (Table 2).

4. Results

4.1 Lithostratigraphy

Our lithostratigraphic survey confirms the complex sequence of minerogenic silts and laterally extensive beds of organic silt that were originally mapped by Smith et al. (2003a). The individual beds onlap the foot of the eastern hillside and can be traced ~100-200 m westward towards the present estuary (Fig. 4) where they mostly dip westward towards the estuary, indicating that the shallower, valley-side sediments are less compacted than those closer to the present estuary. Within the beds and often within overlying minerogenic deposits in small quantities we found macrofossil remains of *Phragmites australis*, a common indicator of a fringing salt-marsh environment (>MHWST) (e.g. Zong and Horton, 1999). The most prominent organic beds (traceable across at least two transects) are those that occur at ~3 m, ~5 m and ~7 m OD which we refer to as 'lower', 'middle' and 'upper' beds, respectively. They are dated in sample core BC421 (Transect 1) to ~8800, ~8200 and ~7800 cal yr BP. The top of the lower and middle beds contain detrital, horizontally-bedded wood fragments that have been transported from the adjacent freshwater upland and are overlain by gray silty clays containing sparse well-humified flecks and minor layers (sub mm) of unidentified organic material. This is evidenced above the middle bed where LOI peaks and remains high across the transition to overlying minerogenic silt. These transitions from organic to minerogenic sedimentation may record evidence of marsh drowning. In contrast, the upper organic bed is overlain by freshwater peat and may record regression. Overall, LOI is high within the organic beds (20-60%) and low within the silts (5-10%; Fig. 6). The elevations of the upper and middle beds can be correlated laterally, although the lower organic bed is not present in the south of the site (Transect 3). There is also stratigraphic variability. For example, there is a locally constrained organic deposit in Transect 2 that rises

from ~7 m OD in the west to ~9 m OD at the valley-side. To provide a rigorous test of hypothesis (1), i.e.; whether RSL rose by more than one abrupt step prior to the 8.2 event, our focus is on the entire sedimentary sequence that embraces the lower and middle organic beds and their overlying minerogenic deposits within core BC421. Later, we discuss the potential regional-global sea-level significance of this depositional sequence.

In the south of Blair's Croft, a gravel barrier underlies the surface peat (Fig. 3). Wells (1997) traced this feature farther north towards the wooded part of Blair's Croft where it falls sharply in altitude and is overlain by minerogenic silts. In Transect 3, the upper organic bed at ~7 m OD is recorded on the landward and seaward sides of the barrier suggesting that it was in place at its present position after the deposition of the upper bed. Two ages from near the base of the upper bed (7917-7608 and 7923-7694 cal yr BP; Fig. 5) thus provide a maximum age of ~8000 cal yr BP of barrier formation, at least at its present position. The potential influence of a palaeo-barrier on the stratigraphy that pre-dates ~8000 cal yr BP is considered later in the discussion.

4.2 Biostratigraphy

In general, the organic beds are dominated by high frequencies of *Navicula peregrina*, a high marsh taxon (Fig. 6), while the minerogenic silts contain *T. navicularis, Nitzschia sigma, Diploneis smithii, Gyrosigma wansbeckii, Cocconeis scutellum* (all epipelic or epiphytic taxa) and *Paralia sulcata* (planktonic), which are indicative of lower intertidal saltmarsh/mudflat conditions. For brevity, epipelic and epiphytic taxa are hereafter collectively referred to as 'benthic'.

The transition between the lower organic bed and the overlying silt is sharp (<2 mm), with the microfossils indicating an abrupt (but non-erosive) switch from high marsh to lower intertidal conditions (Fig. 6). The overlying minerogenic silt contains minor amounts of well-humified organics, including *in situ* roots alongside organic material washed onto the tidal flat from a higher elevation, indicating close proximity of a lower salt marsh environment. At ~530 cm the diatoms begin to record a gradual return to saltmarsh conditions, with *P. sulcata* giving way to increased frequencies of *T. navicularis*. Frequencies of *P. sulcata* undergo a second increase from 30% to 55% between 511 and 494 cm, above which benthic taxa are not present until 455 cm. This section of core is mostly barren, but two samples contain

thickly silicified planktonic taxa *Thalassiosira eccentrica*, *Podosira stillegera*, *Stephanopyxis turris* and *Rhaphoneis amphiceros*. Organic content is low (<3%) and the core log records an increase in clay content. Either side of this planktonic zone, relatively low frequencies of *Cocconeis scutellum* (<10%) indicate a mudflat setting. Overall these data indicate the abrupt drowning of an already low intertidal setting. Higher up in the overlying minerogenic silt between 451 and 414 cm, *D. smithii* and *N. sigma* indicate a gradual return to lower salt-marsh conditions and the establishment of the middle bed.

Accumulation of the middle bed between 414 and 389 cm and the presence of high frequencies of *N. peregrina* indicate a full establishment of high marsh conditions. The contact between the middle bed and overlying minerogenic sediment is sharp (<2 mm), although there are relatively gradual microfossil involving increased frequencies of *T. navicularis*, *P. sulcata* and *D. smithii*. A final return to full high-marsh conditions is indicated by renewed deposition of organic silt at 315 cm which forms the organic silt that underlies peat and contains high frequencies of *N. peregrina* throughout.

In summary, there are three stratigraphic levels that record intertidal drowning within the Blair's Croft stratigraphic record between 8.8 and 7.8 ka BP (Fig. S3). Summarised from bottom to top, these are: i) across the transition between the lower bed and its overlying minerogenic deposit (high marsh drowning), ii) within this overlying minerogenic deposit, across the full length of the 'planktonic zone' (low marsh/mudflat drowning), and, iii) across the transition between the middle bed and its overlying minerogenic deposit (high marsh drowning).

4.3 Transfer function development

We introduce new samples to the Barlow et al. (2013) transfer function to resolve the issue of a missing modern analogue (*T. navicularis*). The species environmental response of the data determines model selection choice; those with environmental gradients >2 standard deviation (SD) units are generally considered to respond unimodally and require a weighted averaging partial least squares (WA-PLS) regression model, while a simple weighted averaging (WA) model is appropriate for datasets with gradient lengths <2 SD (Birks, 1995). The original Barlow et al. (2013) dataset is strongly unimodal (4.08 SD units), which is retained after adding the additional samples from Brancaster Marsh. We therefore use WA-PLS regression

with bootstrapping (1000 permutations) cross validation (ter Braak and Juggins, 1993; Birks, 1995) using the C^2 software v. 1.6 (Juggins, 2011). Fig. S6 and Table S2 (supplementary info) plots observed versus predicted and observed versus residuals of the full dataset, which now includes 27 samples from Brancaster Marsh (total = 231 samples).

To improve the predictive ability of the transfer function, the training set is 'screened' of outlying samples. We follow Gehrels et al. (2005) who discount samples with residuals >1 SD of SWLI, which removes 14 samples, leaving 217 samples. Fig. S6 and Table S3 (supplementary info) illustrates the performance (observed versus predicted and observed versus residual plots) of the one-, two- and three-component models of the screened dataset. We select the WA-PLS model with two components over the one-component model on the basis of an improvement in r^2 and RMSEP by >5% (after Barlow et al., 2013). Good agreement of the Brancaster Marsh samples is indicated by low residuals in the observed versus residual plot (supplementary info Fig. S6; red crosses). Detrended correspondence analysis (DCA) also indicates a good degree of similarity between most of the Brancaster Marsh samples with the pre-existing samples (supplementary info Fig. S7), giving us further confidence in the decision to integrate these samples.

4.4.1 Modern analogues

Integration of the Brancaster Marsh data facilitates the inclusion of *T. navicularis* in the reconstruction but a further 27 taxa remain with no modern analogues (supplementary info Fig. S8). These are rare forms, however, so they have little impact on the reconstruction.

A more important issue, however, concerns the inclusion of *P. sulcata* in the reconstruction, a highly-siliceous planktonic taxon that is present in high abundance in the minerogenic silts and indeed mudflat settings elsewhere in the U.K. (Zong and Horton, 1999; Gehrels et al., 2001; Wilson and Lamb, 2011; Hill et al., 2007). Planktonic taxa are assumed to have an imprecise relationship with RSL because they can be allochthonous (i.e., transported) although in the Cree fossil record, *P. sulcata* demonstrates gradual (linear) changes in abundance across the lithological transitions between organic mud and minerogenic mud. As its ecological optimum occurs around the elevation of the upper tidal flat in the modified Barlow et al. (2013) model, the ecological information on its distribution appears to be supported by stratigraphic changes. If not directly controlled by elevation, the

distribution of *P. sulcata* likely reflects other processes that are tightly coupled to elevation such as increased/decreased tidal influence. This presents a problem as we are unable to test the robustness of the ecological optimum of *P. sulcata* in the modified Barlow et al. (2013) model. However, we have no choice but to include it in the reconstruction as it provides constraints on the indicate meanings of tidal flat deposits and extends the vertical range of our reconstruction to these environments, which are critical to constraining a minimum magnitude of drowning events (i.e., abrupt transitions from organic to minerogenic sedimentation). In doing so we recognise that accurately interpreting genuine short-lived events within our reconstruction requires careful consideration of the assemblage contributions of *P. sulcata* and whether these are supported by lithostratigraphic and additional biostratigraphic information. This issue is further addressed in Section 5 (Discussion).

4.4 Chronology

The chronology is based on nine tie-points (a total of 13 AMS ^{14}C ages, including a mixture of duplicate and single dates) that are modelled in stratigraphic sequence in OxCal v 4.2 (Bronk Ramsey, 2009a) (Fig. S4). The model builds prior (unmodelled) probability distributions of ^{14}C ages and compares them with posterior (modelled) densities using Bayesian analysis and Monte Carlo Markov Chain random sampling (Gilks et al., 2006). The agreement index provides a measure of overlap between the prior and posterior model densities, with agreement indices >60% the accepted threshold (Bronk Ramsey, 2008). In our model, there is good agreement between the prior and posterior densities; seven out of eight tie-points have an agreement index of >77%, while the one remaining tie-point has a satisfactory agreement of 61%. Posterior probability densities for each RSL (y) data-point were determined by inserting blank ages into the model at the relevant stratigraphic position using the Date() function. Finally, we introduce the assumption that organogenic and minerogenic sequences accumulate at different rates by introducing 'boundaries' at organic – minerogenic stratigraphic contacts as without their introduction we were unable to model the sequence with a satisfactory level of agreement.

4.5 Sea-level reconstruction

Prior to undertaking any probabilistic analysis of our fossil record we describe the reconstruction in its raw form. Fig. S10 plots transfer function output (SWLI) versus both depth (Fig. S10a) and modelled ages (Fig. S10b). The full dataset is presented in Table S1. We identify two sustained reductions in palaeo-marsh surface elevation that support our preliminary interpretations of marsh drowning based on biostratigraphy alone. The first (lowest) is between 627 cm (8791-8531) (all ages 2σ with respect to cal yrs BP) and 610 cm (8850-8528) and corresponds stratigraphically with the transition between the lower organic bed and overlying minerogenic deposit. The second is found between 511 cm (8621-8381) and 445 cm (8497-8321) and reflects the minerogenic section of core dominated by planktonic taxa, which are under- and overlain by relatively high occurrences of benthic lower marsh taxa ('the planktonic zone') (Section 4.2). The upper section of the core contains a period of lower amplitude changes in SWLI albeit superimposed on a highly fluctuating record. Within this section we note the possible existence of a third event at the level that corresponds across the broad transition between the middle organic bed and overlying clay between 395 cm (8353-8229) and 360 cm (8227-8087) and registered as a sub-centennial scale period of lower amplitude SWLI oscillations.

Following transformation of the SWLI values to sea level we are now in a position to assess the evidence of marsh drowning probabilistically (Table S2). Fig. 7b shows the probabilistically determined RSL reconstruction in the Cree Estuary for the period 8800 to 7800 cal yr BP. The reconstruction shows RSL rising around 3 mm/yr from 8800 to 8000 cal yr BP and a slowdown from 8000 to 7800 cal yr BP. The relatively wide 1σ and 2σ confidence intervals reflect the sensitivity of the random sampling technique to uncertainties in time and space.

A number of low amplitude (decimetre-scale) sea-level changes are evident in the reconstruction, superimposed upon the millennial scale background trend. To isolate these deviations, we use the independent RSL reconstruction for the Cree Estuary of Bradley et al. (2011) as a threshold above which a sea-level event may be defined. This curve is derived from a solution to the sea-level equation (Mitrovica & Milne, 2003) with an updated deglacial history for the British and Irish Ice Sheet. The proximity of the site to the former centre of this ice sheet means that it is strongly affected by glacial isostatic adjustment, which is recorded in the RSL record. Since the Bradley et al. (2011) reconstruction is sampled at

1000 year time steps we choose to use this as our background sea-level curve. Using this background curve (and the rate one obtains by differentiating it) is a more conservative approach than using quadratic or cubic polynomials (e.g. Milliken et al., 2008) or partial linear segments either side of supposed sea-level jump (e.g. Hijma & Cohen, 2010) because it does not rely upon the RSL data itself to ascertain a background rate.

Fig. 7a plots rates of RSL change derived using the two methods outlined in Section 3.4 (dataset presented in Table S3). For both mean RSL rate reconstruction ($\mu_{dRSL/dt}$) and differentiated mean RSL reconstruction ($d\mu_{RSL}/dt$) we observe a centennial-scale increase in the rate of RSL between ~8700-8300 cal yr BP that exceeds the background trend as defined by the Bradley et al. (2011). The fine structure of these differentiated records allow this event to be separated into two episodes, with a first commencing at ~8700 cal yr BP and a second at ~8560 cal yr BP. Third, we observe relatively minor fluctuations in rates of rise beyond the background threshold between the 8250-8150 cal yr BP time period. Importantly, these events correspond in time to the increases in SWLI within the raw reconstruction data and can therefore not be considered artefacts of the probabilistic assessment.

Determining precise estimates of the timing and magnitude of sea-level changes in the critical interval is difficult given the nature of our dataset and its uncertainties. Clear limitations exist in developing sub-centennially resolved sea-level histories from macrotidal settings, since the uncertainties in transfer-function derived RSL reconstructions are typically 10% of the tidal range (Barlow et al., 2013). Each RSL data point also accounts for uncertainties relating to palaeotidal change (± 0.2 m) and compaction (± 0.2 m). Nevertheless we choose to proceed with reconstructing the timing and magnitudes of these events more precisely, using data around the mean, given the compelling evidence of marsh drowning within the stratigraphy. To achieve this, we utilise our differentiated RSL curves ($d\mu_{RSL}/dt$).

Here we test hypothesis (1) with the following criterion: where rates of rise in the three differentiated RSL curves ($d\mu_{RSL}/dt$, $d(\mu-\sigma)_{RSL}/dt$, $d(\mu+\sigma)_{RSL}/dt$) exceed the background rate (Bradley et al. 2011). The crossing time of each differentiated curve allows a simple range to be calculated for the onset of a sea-level event. Applying this criterion, we identify three accelerations in the rate of RSL rise (Table 3). The first occurred between 8760-8640 cal yr BP and registered a sea-level jump of 0.24-0.45 m ($RSLr_1$), while the second was at 8595-8465 cal yr BP and registered 0.67-0.73 m ($RSLr_2$). The final event registered 0.37-0.43 m of sea-level rise within the period 8320-8235 cal yr BP (all ranges are 3σ of the differentiated series).

We establish the total mass loss from each of these events by scaling the associated local RSL change by the percentage of global sea-level (GSL) equivalent predicted by Kendal et al. (2008) at the measurement site (Table 2). We perform this scaling by assuming a North American source (Fig. 1) and that the sea-level fingerprint is invariant to the magnitude of mass change so long as the geometry is the same. While in the Cree Estuary and Rhine-Meuse Delta, RSL is predicted to record 70% of the GSL equivalent change, the Mississippi Delta RSL would only record 20%.

5. Discussion

5.1 Assessing the evidence for sea-level jumps in the Blair's Croft record

We infer the RSL significance of abrupt microfossil changes by considering supporting (stratigraphic) evidence of abrupt drowning and whether these could reflect local morphodynamical processes. In turn, we assess the global sea-level significance of the Cree observations.

On the basis that abrupt microfossil changes are supported by lithostratigraphic evidence, in particular abrupt switches from organogenic to minerogenic sedimentation, we accept $RSLr_1$ and $RSLr_3$ as significant RSL jumps (Table 3). The notion that $RSLr_2$ is a genuine short-lived event rests heavily on the interpretation of the relatively barren 'planktonic zone'; a 45 cm unit containing only two samples of planktonic microfossils. Critically, the stratigraphy below the planktonic zone contains evidence of minor marsh recovery in the form of increased abundance of well-humified organic macrofossils and is in line with the interpretation that our marsh was experiencing recovery after a preceding sea-level jump ($RSLr_1$). We therefore interpret the overlying planktonic zone as a drowning of a high mudflat or lower salt marsh environment that was in the early stages of vegetational recolonization. Moreover, our decision to introduce 'boundaries' within the age model at organogenic-minerogenic contacts will not have influenced the results from this section of core. Secondly, low marsh benthic microfossils (*Cocconeis scutellum*) increase in abundance immediately above and below the planktonic zone, demonstrating that accumulation kept pace within a sustained, sub-centennial to multi-decadal period where accommodation space was made available. In turn this line of evidence is not consistent with the notion that tidal

scour or a high-energy event such as a storm (e.g. Haslett and Bryant, 2007) as the microfossil record reflects gradual changes instead of abrupt transitions associated with erosion (Fig. 6). Third, supporting evidence of lagoonal infilling in response to enhanced freshwater runoff, such as laminations or freshwater taxa, are not present either within or above and below this unit. A further key observation is provided by Smith et al. (2003a), who describe an unprecedented increase in clay content at Carsewalloch Flow towards the centre of the estuary (Fig. 3C) between 4.0-4.5 m OD. Its elevation is similar to the elevation of the planktonic zone in BC421 (4.90-4.45 m OD) albeit slightly lower, likely reflecting less compaction of the valley side sediments at our site. We therefore suggest that the planktonic zone in BC421 records a shift in sedimentology that extends beyond Blair's Croft towards the centre of the estuary. We propose that the lack of a distinct organogenic-minerogenic lithostratigraphic signature similar to that observed for $RSLr_1$ and $RSLr_3$ can be explained by the low intertidal height of the pre-drowned surface (high mudflat or low salt marsh). The Solway Firth and its sub-estuaries contain an abundance of fine-grained sediment, which likely supported rapid sedimentation once accommodation space was made available by sudden sea-level rise. On these grounds, we conclude that there is strong evidence that $RSLr_2$ was a genuine RSL jump.

There are other possible explanations for the drowning events identified in the Blair's Croft sequence that could be of local origin and which require consideration. First, meandering tidal creeks could alter the local depositional environment and result in changes in diatom assemblages within the sample core. We dismiss this possibility on the basis that channel deposits are usually distinct within the litho- and biostratigraphy (e.g. Long and Innes, 1993; Zecchin et al., 2014) and do not operate over the wide areas in which the Blair's Croft organic beds are observed. A second possibility is that the local site stratigraphy may record changes in coastal morphodynamics associated with the development of a coastal barrier. This is potentially important when considering the RSL significance of the final event ($RSLr_3$), which is derived from an exceptionally noisy part of the record. The site-wide stratigraphy that overlies this upper section of core is complex, with interweaving organic-minerogenic deposits that cannot be traced laterally in all cores. As noted above, the site chronology indicates that a gravel barrier was deposited at its present position sometime before c. 8000 cal yr BP. We find no stratigraphic evidence for changes in the dynamics of this barrier during the timeframe of our record, such as barrier over-wash deposits or evidence for tidal inlet deposition. However, we cannot rule out the control of barrier morphodynamics on the development of the latter stages of the record. For instance, Smith et

al. (2003a) describe evidence of a further two barrier ridges on the opposite side of the estuary of a similar morphology and this probably attests to the abundance of glacial sediment now buried within the valley lowlands. By the same token, a gravel barrier at the site would have provided a degree of protection for low energy conditions in its lee after c. 8000 cal yr BP until the culmination of the RSL highstand in the region.

A final observation is that rates of RSL rise determined from sediments across the middle and upper organic beds are low. There is a gradual slowdown in the rate of long-term RSL rise across the interval that eventually falls short of the background trend as derived from Bradley et al. (2011) model. Plausibly, this might be explained by the long-term overburden pressure and the reduction in the thickness of the organic beds, suggesting that estimates of RSL rise may be underestimated. As organic (saltmarsh) sediments experience a greater degree of compressibility than minerogenic (mudflat) sediments (e.g., Brain et al. 2011) we can assume that $RSLr_2$ is unaffected by the impact of compression variability across lithologies as it is recorded within a single minerogenic silt. On the other hand, $RSLr_1$ and $RSLr_3$ directly overlie the lower and middle beds and their onsets occur at or near the organogenic-minerogenic contacts. Whilst we cannot quantify the influence of compaction, the microfossil changes observed are independent of potential compaction variability across lithologies. Hence, we conclude that there is evidence that RSL rose in three steps prior to the 8.2 event and are therefore unable to reject hypothesis (1), that RSL rose in more than one abrupt step in the centuries leading up to the 8.2 event.

5.2 Comparison with existing chronologies: testing hypothesis (2)

There is debate regarding the potential routing and impact of freshwater discharge at the time interval of interest, with some authors suggesting routing into the sub-tropical North Atlantic and not the sub-polar gyre (e.g. Condron and Windsor 2011; Hill and Condron, 2014). Nevertheless, the strong polar foraminiferal and $\delta^{18}O$ signal in records from the sub-polar North Atlantic (Ellison et al., 2005; Kleiven et al., 2008) indicates a significant impact in this region and provides a basis for chronological comparison with the three Cree Estuary RSL jumps.

Fig. 8 plots the age probability density functions and 2σ ranges (bars) computed for the start of each respective North Atlantic event. We observe ages that cluster in three largely

distinct time intervals, with mid-points that are separated by up to two centuries. A first group contains $RSLr_1$, DCP6a and modelled peak meltwater discharge concomitant with LIS saddle collapse, which all occur between ~8800 to ~8600 cal yr BP. A second group of events contains $RSLr_2$, DCP6b; the downstream equivalent of the Hudson Bay "red-bed", the Rhine-Meuse Delta RSL jump and the earliest North Atlantic surface freshening event (FE_1) in MD99-2665, which occur between ~8600 to ~8300 cal yr BP. The final group of events occurred between ~8300 and ~8100 cal BP, where $RSLr_3$, the Mississippi Delta RSL jump and the youngest North Atlantic surface freshening event (FE_2) in MD99-2665 indicate strong overlap at the 1σ probability level. The 2σ range of DCP7 (Jennings et al., 2015) and the LAO drainage deposit recorded in James Bay (Roy et al., 2010) overlaps with the 2σ range of this final age group. In addition, they all overlap with the start of the 8.2 event at 8247 cal yr BP (Thomas et al. 2007). Table 2 provides the age determinations of these individual estimates.

Interpreting an accurate sequence of freshwater events is strongly dependent on the accuracy of the underpinning chronologies. Maximising chronological accuracy and precision is critical given the short timescale under consideration and because of the limitations imposed by variable ^{14}C production across the time interval. In particular, minor plateaus in ^{14}C production occur between 8550-8400, 8300-8200 and 8150-8050 cal yr BP, while a much larger plateau occurs at 8950-8650 cal yr BP and could be implicated in the strong correlations in Fig. 8. To some extent however, this potential biasing effect is mitigated where age models incorporate stratigraphic information; such is the case with the Cree record. However, our age model contains the assumption that sharp changes from organic to minerogenic sedimentation reflect a changing rate of accumulation. Our introduction of "boundaries" at these contacts effectively forces the model to derive a solution that is otherwise not possible given our dating constraints and nature of the stratigraphic sequence. Validation of our observations is therefore required, especially with respect to time constraints. As a final point, the estimates derived from marine chronologies presented here depend strongly on the magnitude of local marine reservoir corrections which are difficult to define. These limitations are inherent to the process of ^{14}C calibration but are compounded when working on these timescales. Notwithstanding these issues we suggest that events are likely to have been interrelated in some way when ages overlap, especially at the 1σ probability level.

The Cree observations demonstrate significant overlap in timing with existing estimates of short-lived events (Fig, 8); in particular those within the best resolved near-field record of final LIS retreat on the Cartwright Saddle (Jennings et al., 2015), but also from the two existing RSL records that span the critical time interval. After correcting $RSLr_1$ and $RSLr_2$ for a Laurentide source of freshwater release, $RSLr_1$ measured 0.35-0.65 m while $RSLr_2$ measured 0.96-1.04 m. This is in good agreement with the fingerprint-corrected sea-level jump observed in the in the Rhine-Meuse Delta of 3.0 ± 1.3 m (1σ; Hijma and Cohen, 2010). It has been speculated that the Rhine-Meuse RSL jump records two or more distinct events (Hijma and Cohen, 2010; Li et al., 2012), a suggestion that is in agreement with our data after considering the magnitudes of $RSLr_1$ and $RSLr_2$ once combined (1.92-2.23 m) (Table 2). Thus, there is compelling evidence to support an interpretation that two episodes of freshwater release occurred in quick succession, and that these their distinct separation has yet to be fully detected in the Rhine-Meuse Delta sea-level record (Hijma and Cohen, 2010). Finally, the magnitude of $RSLr_3$ once corrected for a Laurentide source of freshwater release (0.54-0.61 m) is in good agreement with the magnitude of the fingerprint-corrected RSL jump identified in the Mississippi Delta (0.3 ± 0.3 m; 2σ; Li et al., 2012) .

5.3 Deriving a sequence of events between 8900 to 8200 cal yr BP

In light of the Cree and existing observations, we propose the following three-event model of freshwater forcing from the LIS between 8900-8200 cal yr BP.

First, collapse of the Keewatin and Labrador ice-dome saddle (Gregoire et al., 2012) was swiftly followed by the opening of the Tyrrell Sea (Jennings et al., 2015). It coincides closely with detrital carbonate event DCP6a in core MD99-2236 from the Cartwright Saddle, dated to 8694-8609 cal yr BP (Jennings et al. 2015). This first event at ~8700 cal yr BP registered a RSL rise in SW Scotland of 0.25-0.45 m, which translates to a eustatic-equivalent magnitude of 0.35-0.65 m. There is no evidence of this event within sub-polar North Atlantic proxy records which could reflect low rates of freshwater discharge during this event, relative to the events that followed. However, it overlaps with a possible cold event at 8.75 ka BP exemplified by Rasmussen et al. (2007) in Greenland ice-core records. It could also have been responsible for the onset of the broad climatic anomaly that starts around this time (Rohling and Pälike, 2005).

A second episode of enhanced freshwater forcing followed shortly after at ~8560 cal yr BP and this registered a surface and deep ocean signal (FE_1; Kleiven et al., 2008; Ellison et al., 2005 Fig. 2) along with RSL jumps in SW Scotland ($RSLr_2$) and the western Netherlands. It was likely responsible for the reworked stratigraphy in the Mississippi Delta record (Li et al., 2012). The event agrees in timing with DCP6b, which Jennings et al. (2015) date to 8609-8489 cal yr BP and correlate with the Hudson Bay "red bed" deposit (e.g. Barber et al., 1999). We propose that $RSLr_2$ records the first and largest drainage of LAO. As it swiftly followed $RSLr_1$, we suggest that the collapse of the Keewatin and Labrador ice-domes reached a critical threshold whereby sufficient thinning forced the drainage of LAO subglacially under buoyant ice (Lajeunesse and St Onge, 2008; Clarke et al., 2004; Teller et al., 2002). The notion of a negligible time gap between these two events is supported by two lines of evidence; first, DCP6 has been subdivided into two remarkably close but largely separate events (DCP6a and DCP6b) by Jennings et al. (2015). Second, the Rhine-Meuse Delta RSL record (Hijma and Cohen, 2010) was unable to capture two distinctly separate events.

The final event within the Cree Estuary ($RSLr_3$) occurred between 8323-8218 cal yr BP and correlates broadly with DCP7; dated to 8219-7998 cal yr BP, which Jennings et al. (2015) interpret as representing the possible two-staged release of LAO and the cause of the 8.2 event. The LIS was the most likely source of this event given its registration in sub-polar North Atlantic proxy records (Ellison et al. 2006; Kleiven et al., 2008). It is therefore unlikely that the majority of freshwater was routed south into the sub-tropical gyre (Condron and Windsor, 2011; Hill and Condron, 2014), although it remains possible that this region received a portion of the total discharge volume. In view of the James Bay drainage deposits, which provide strong overlap at the 1σ probability level (Roy et al. 2011), we interpret this event as the second and final drainage of LAO following a century-scale phase of partial lake recharge (Teller et al., 2002).

The differences in the magnitudes of RSL jumps have implications for AMOC sensitivity. The relatively large and abrupt freshwater pulses at ~8700 and ~8560 cal yr BP associated with the opening of the Tyrrell Sea and first drainage of LAO respectively could have preconditioned the AMOC (e.g. Carlson and Clark, 2012), with a relatively modest freshwater perturbation at ~8270 yrs BP triggering its eventual reorganization. Thereafter, it is possible that sea-ice-albedo feedbacks (Wiersma and Jongma, 2010; Otto-Bliesner and

Brady, 2010) and freshwater fluxes were important in forcing the 8.2 event (Teller et al., 2002; Törnqvist and Hijma, 2012).

6. Conclusions

The exceptionally well-mapped 8.2 event was originally thought to have been triggered by an AMOC freshwater perturbation associated with the drainage of LAO, but studies based on empirical data and modelling have increasingly speculated that the single-event model of freshwater forcing is an oversimplification of the 8.2 event's causal mechanism. RSL records provide one of the few means to calculate the magnitude of freshwater released and to determine a likely sequence of freshwater events prior to the 8.2 event.

We present the first microfossil-based RSL record that is continuous from 8800 to 7800 cal yr BP. It contains three decimetre- to metre-scale RSL jumps that overlap in age with a range of abrupt events expressed in existing North Atlantic records, lending significant support to a three-event model of Laurentide freshwater release within the c. 500 yr window prior to the 8.2 event.

Our observations agree with a two-event model of LAO drainage which was preceded by a dynamical ice-sheet contribution at ~8650 cal yr BP (0.35-0.65 m). The first (penultimate) drainage was at ~8565 cal yr BP (0.96-1.04 m), while the final appears coeval with the start of the 8.2 event. Our observations demonstrate the potential offered by integrating ice core, ocean and coastal records of environmental change across this turbulent interval of the Holocene, whilst also highlighting the challenges posed by developing continuous records from single stratigraphic sequences that rely heavily on the radiocarbon method. Developing additional highly resolved RSL records of the type developed here, preferably from low tidal range settings and from southern Hemisphere settings to assist in fingerprinting sources and magnitudes of sea-level change, will enable further testing of the hypotheses that lie at the heart of this study.

Acknowledgements

Funding for this work was provided by a Durham Doctoral Award to TL. Hatfield College and the Hatfield College Trust are kindly acknowledged for fieldwork support. Radiocarbon

dating support comes from the Natural Environmental Research Council Radiocarbon Committee, allocation #1629.0312. We thank Drs. Sarah Bradley, Anne Jennings and Sophie Ward for providing and discussing various datasets and Professor Eelco Rohling for clarifying the probabilistic assessment method. This work benefitted from discussions with Drs. Lauren Gregoire, Sarah Woodroffe, James Wells and Professor Ian Shennan. We are grateful to Scott Rexworthy and Josh Kittlety for their assistance in the field and Mervyn Brown, Frank Davies, Alison George and Kathryn Melvin for technical and laboratory assistance. The reviews of Professor Torbjorn Törnqvist and an anonymous reviewer greatly improved an earlier version of the manuscript. This paper is a contribution to PALSEA2, IGCP 588 and the INQUA Commission on Coastal and Marine Processes.

References

Alley, R. B., P. A. Mayewski, T. Sowers, M. Stuiver, K. C. Taylor, and P. U. Clark (1997), Holocene climatic instability: A prominent, widespread event 8200 yr ago, *Geology* **25**, 483–486.

Alley, R.B and Agustdottir, A.M. 2005. The 8k event: causes and consequences of a major Holocene abrupt climate change, *Quaternary Science Reviews* **24**, 1123-1149.

Barber, D.C., Dyke, A., Hillaire-Marcel, C., Jennings, A.E., Andrews, J.T., Ker- win, M.T., Bilodeau, G., McNeely, G., Southon, J., Morehead, M.D., and Gagnon, J.-M. 1999. Forcing of the cold event of 8,200 years ago by catastrophic drainage of Laurentide lake: *Nature* **400**. 344–348, doi: 10.1038/22504.

Barlow N. L. M., Shennan I., Long A.J., Gehrels, W.R., Saher, M.H., Woodroffe, S.A., Hillier, C. H. 2013. Salt marshes as late Holocene tide gauges. *Global and Planetary Change* **106**, 90–110.

Birks, H.J.B., 1995. Quantitative palaeoenvironmental reconstructions. In: Maddy, D., Brew, J.S. (Eds.), Statistical Modelling of Quaternary Science Data. Quaternary Research Association, Cambridge, 161–254.

Bishop, W. W. & Coope, G. R. 1977. Stratigraphical and faunal evidence for Lateglacial and early Flandrian environments in south-west Scotland. In Gray, J. M. & Lowe, J. J. (eds), *Studies in the Scottish Late glacial environment*, 61±88. Oxford: Pergamon Press.

Bondevik, S., Stormo, S.K., Gudrun, S. 2012. Green mosses date the Storegga tsunami to the chilliest decades of the 8.2 ka cold event, *Quaternary Science Reviews* **45**, 1-6. doi:10.1016/j.quascirev.2012.04.020.

Bradley, S.L., Milne, G.A., Shennan, I., and Edwards, R. 2011. An improved Glacial Isostatic Adjustment model for the British Isles, *Journal of Quaternary Science* **26**, 5, 541-552.

Brain, M.J., Long, A.J., Petley, D.N., Horton, B.P. and Allison, R.J. Compression behaviour of minerogenic low energy intertidal sediments. *Sedimentary Geology* **233**, 28-41.

Bronk Ramsey, C. 2000. Comment on 'The Use of Bayesian Statistics for 14C dates of chronologically ordered samples: a critical analysis'. *Radiocarbon, **42***, 2, 199-202.

Bronk Ramsey, C. 2008. Deposition models for chronological records. *Quaternary Science Reviews, **27***, 1-2, 42-60.

Bronk Ramsey, C. 2008. Deposition models for chronological records. *Quaternary Science Reviews, **27***, 1-2, 42-60.

Bronk Ramsey, C. 2009. Bayesian analysis of radiocarbon dates. *Radiocarbon, **51***, 1, 337-360.

Carlson, A.E., and Clark, P.U., 2012, Ice-sheet sources of sea-level rise and freshwater discharge during the last deglaciation, *Reviews of Geophysics* **50**, doi: 10.1029/2011RG000371.

Clarke, G. K. C., Leverington, D. W., Teller, J. T. & Dyke, A. S. 2004. Paleohydraulics of the last outburst flood from glacial Lake Agassiz and the 8200 BP cold event. *Quaternary Science Reviews* **23,** 389–407.

Condron, A., Windsor, P. 2011. A subtropical fate awaited freshwater discharged from glacial Lake Agassiz, *Geophysical Research Letters* **38**, 3, 10.1029/2010GL046011.

Cullingford, R. A., Caseldine, C. J. and Gotts, P. E. 1980. Early Flandrian land and sea level changes in Lower Strathearn. *Nature* **284**, 159-61.

Czernik, J., Goslar, T. 2001. Preparation of graphite targets in The Gliwice Radiocarbon Laboratory for AMS 14C dating. *Radiocarbon* **43**, 283–291.

de Vernal, A., Hillaire-Marcel, C., von Grafenstein, U., Barber, D., 1997. Researchers look for links among paleoclimate events: EOS (Transactions, American Geophysical Union) **78**, 247–249.

Ellison, C.R.W., Chapman, M.R., and Hall, I.R. 2006. Surface and deep ocean interactions during the cold climate event 8200 years ago. *Science* **312**, 1929–1932, doi: 10.1126/science.1127213.

Gehrels W.R., Kirby J.R., Prokoph A., *et al.* 2005. Onset of recent rapid sea-level rise in the western Atlantic Ocean. *Quaternary Science Reviews* **24**: 2083–2100.

Gehrels, W.R., Roe, H.M., Charman, D.J. 2001. Foraminifera, testate amoebae and diatoms as sea-level indicators in UK saltmarshes: a quantitative multiproxy approach, *Journal Quaternary Science* **16**, 3, 201-220. DOI: 10.1002/JQS.588.

Gilks, W., Richardson, S., Spiegelhalter, D. (Eds.) 1996. Markov Chain Monte Carlo in Practice. Chapman & Hall, London.

Gregoire, L. J., Payne, A. J., Valdes, P. J. 2012. Deglacial rapid sea level rises caused by ice-sheet saddle collapses, *Nature* **487,** 219–222.

Hartley, B., Barber, H.G., Carter, J.R. 1996. An Atlas of British Diatoms. Sims, P.A (ed). Biopress, London.

Haslett, S.K., and Bryant, E.A. 2007. Reconnaissance of historic (post-AD 1000) high-energy deposits along the Atlantic coasts of southwest Britain, Ireland and Brittany, France. *Marine Geology* **242**, 207-220.

Hijma, M.P and Cohen, K.M. 2010. Timing and magnitude of the sea-level jump precluding the 8200 yr event, *Geology* **38**, 3, 275-278.

Hill, J.C., Condron, A. 2014. Subtropical iceberg scours and meltwater routing in the deglacial western North Atlantic, *Nature Geoscience* **7**, 806-810. DOI: 10.1038/NGEO2267.

Hill, T.C.B., Woodland, W.A., Spencer, C.D., and Marriot, S.B. 2007. Holocene sea-level change in the Severn Estuary, southwest England: a diatom-based sea-level transfer function for macrotidal settings. *The Holocene*, **17**, 5, 639-648.

Hillaire-Marcel, C. de Vernal, A. Piper, D.J.W. 2007. Lake Agassiz final drainage event in the North Atlantic. *Geophysical Research Letters* **34**, doi:10.1029/2007GL030396.

Hoffman, A.S., Carlson, A.E., Windsor, K., Klinkhammer, G.P., Le Grande, A.N., Andrews, J.T., Strasser, J.C. 2012. Linking the 8.2 ka event and its freshwater forcing in the Labrador Sea, *Geophysical Research Letters* **39**, doi:10.1029/2012GL053047.

Hydrographic Office (2011) Admiralty Tide Tables: United Kingdom and Ireland including European and Channel Ports: Hydrographer of the Navy, Taunton, Somerset, 1, 1-364.

Jardine, W. G. 1975. Chronology of Holocene marine transgression and regression in south-western Scotland. *Boreas* **4**, 173 96.

Jennings, A., Andrews, J., Pierce, C., Wilson, L., Olfasdotttir, S. 2015. Detrital carbonate peaks on the Labrador shelf, a 13e7 ka template for freshwater forcing from the Hudson Strait outlet of the Laurentide Ice Sheet into the subpolar gyre, *Quaternary Science Reviews* **107**, 62-80. http://dx.doi.org/10.1016/j.quascirev.2014.10.022.

Juggins, S. (2011) C^2 Version 1.6: Software for Ecological and Palaeoecological Data Analysis and Visualisation: Department of Geography, University of Newcastle, Newcastle upon Tyne, U.K.

Kendall, R.A, Mitrovica, J.X., Milne, G.A., Tornqvist, T.E. and Li, Y.X. 2008. The sea-level fingerprint of the 8.2 ka event, *The Geological Society of America* **35**, 5, 423-426.

Kleiven, H.F., Kissel, C., Laj, C., Ninnemann, U.S., Richter, T.O., Cortijo, E. 2008. Reduced North Atlantic deep water coeval with the glacial Lake Agassiz Freshwater Outburst. *Science* **319**, 5859, 60-64.

Kobashi, T., Severinghaus, J.P., Brook, E.J., Barnola, J.M., and Grachev., A.M. 2007. Precise timing and characterization of abrupt climate change 8200 years ago from air trapped in polar ice. *Quaternary Science Reviews* **26**, 1212–1222, doi:10.1016/j.quascirev.2007.01.009.

Kuchar, J., Milne, G., Hubbard, A., Patton, H., Bradley, S., Shennan, I., and Edward, R. 2012. Evaluation of a numerical model of the British-Irish ice sheet using relative sea-level data: implications for the interpretation of trimline observations, *Journal Quaternary Science* **27**, 6, 597-605.

Lajeunesse, P., and St-Onge, G. The subglacial origin of the Lake Agassiz-Ojibway final outburst flood, *Nature Geoscience* **1**, 184-187. doi:10.1038/ngeo130.

LeGrande, A.N., Schmidt, G.A., Shindell, D.T., Field, C.V., Miller, R.L., Koch, D.M., Faluvegi, G. and Hoffman, G. 2006. Consistent simulations of multiple proxy responses to an abrupt climate change event, *Proceedings of the National Academy of Sciences* **103**, 4, 837-842. doi: 10.1073/pnas.0510095103.

Leverington, D. W., J. D. Mann, and J. T. Teller. 2002. Changes in the bathymetry and volume of glacial Lake Agassiz between 9200 and 7700 14C yr B.P. *Quaternary Research* **57**, 244–252.

Li, Y.X., Tornqvist, T.E., Nevitt, J.M., and Kohl, B. 2011. Synchronizing a sea-level jump, final lake Agassiz drainage and abrupt cooling 8200 years ago, *Earth and Planetary Science Letters* **315-316**, 41-50.

Lloyd,, J.M., Shennan, I., Kirby, J.R. and Rutherford, M.M. 1999. Holocene relative sea – level changes in the inner Solway Firth. *Quaternary International* 60, 83-105.

Long, A.J. and Innes, J.B. 1993. Holocene sea-level and coastal sedimentation in Romney Marsh, southeast England, UK.*The Proceedings of the Geologists' Association*, 104, 223-237.

Marshall, W.A., Gehrels, W.R., Garnett, M.H., Freeman, S.P.H.T., Maden, C., Xu, S., 2007. The use of 'bomb spike' calibration and high-precision AMS 14C analyses to date salt-marsh sediments deposited during the past three centuries. *Quaternary Research*, **68**, 325–337.

Mitrovica, J.X., Gomez, N., Clark, P.U. 2009. The sea-level fingerprint of West Antarctic collapse, *Science* **323**, 753.

Mitrovica, J.X. and Milne, G.A. 2003. On post-glacial sea level: I. General theory. Geophysical Journal International, 154: 253–267. doi: 10.1046/j.1365-246X.2003.01942.x

Mitrovica, J.X., Tamisiea, M.E., Davis, J.L., Milne, G.A. 2001. Recent mass balance of polar ice sheets inferred from patterns of global sea-level change, *Nature* **409**, 1026-1029.

Morrill, C., Ward, E.M., Wagner, A.J., Otto-Bliesner, B.L., Rosenbloom, N. 2014. Large sensitivity to freshwater forcing location in 8.2 ka simulations. *Paleoceanography* **29**, doi:10.1002/2014PA002669.

Otto-Bliesner, B.I. and Brady, E.C. 2010. The sensitivity of the climate response to the magnitude and location of freshwater forcing: last glacial maximum experiments, *Quaternary Science Reviews* **29**, 56-73.

Palmer, A.J.M., and Abbott, W.H. 1986. Diatoms as sea-level indicators. In: Van de Plassche O (ed) Sea level research: A manual for the collection and evaluation of data. Geo Books, Norwich.

Rasmussen, S. O., Seierstad, I. K., Andersen, K. K., Bigler, M., Dahl-Jensen, D., and Johnsen, S. J 2008. Synchronization of the NGRIP, GRIP, and GISP2 ice cores across MIS 2 and palaeoclimatic implications, *Quaternary Science Reviews* **27**, 18–28, doi:10.1016/j.quascirev.2007.1001.1016.

Reimer, P. J., Bard, E., Bayliss, A., Beck, J. W., Blackwell, P. G., Bronk Ramsey, C., Grootes, P. M., Guilderson, T. P., Haflidason, H., Hajdas, I., HattŽ, C., Heaton, T. J., Hoffmann, D. L., Hogg, A. G., Hughen, K. A., Kaiser, K. F., Kromer, B., Manning, S. W., Niu, M., Reimer, R. W., Richards, D. A., Scott, E. M., Southon, J. R., Staff, R. A., Turney, C. S. M., & van der Plicht, J. 2013. IntCal13 and Marine13 Radiocarbon Age Calibration Curves 0-50,000 Years cal BP, *Radiocarbon **55***.

Rohling, E.J., Foster, G.L., Grant, K.M., Marino, G., Roberts, A.P., Tamisiea, M.E. and Williams, F. 2014. Sea-level and deep-sea temperature variability over the past 5.3 million years, *Nature* **508**, 477-482.

Roy, M., Dell'Oste, F., Veillette, J.J., de Vernal, A., Helie, J.-F., Parent, M., 2011. Insights on the events surrounding the final drainage of Lake Ojibway based on James Bay stratigraphic sequences. *Quaternary Science Reviews* **30**, 682-692.

Simkins, L.M., Simms, A.R., Cruse, A.M., Troiani, T. Atekwana, E.A., Puckette, J., Yokayama, Y. 2012. Correlation of early and mid-Holocene events using magnetic susceptibility in estuarine cores from bays along the northwestern Gulf of Mexico, *Palaeogeography, Palaeoclimatology, Palaeoecology* **346-347**, 95-107.

Smith, D.E., Wells, J.M., Mighall, T.M., Cullingford, R.A., Holloway, L.K., Dawson, S., Brooks, C.L. 2003a. Holocene relative sea levels and coastal changes in the lower Cree valley and estuary, SW Scotland, UK. *Transactions of the Royal Society of Edinburgh: Earth Sciences*, **93,** 301-331.

Smith, D.E., Haggart, B.A., Cullingford, R.A., Tipping, R.M., Wells, J.M., Mighall, T.M. and Dawson, S. 2003b. Holocene relative sea level change in the lower Nith valley and estuary. *Scottish Journal of Geology* 39, 97-120.

Smith, D.E., Harrison, S. and Jordan, J.T. 2013. Sea level rise and submarine mass failures on open continental margins. *Quaternary Science Reviews* 82, 93-103.

Tamisiea ME, Mitrovica JX, Milne GA, Davis JL. 2003. Long wave length sea level and solid surface perturbations driven by polar ice mass variations: fingerprinting Greenland and Antarctic Ice Sheet flux. *Space Science Reviews* (108) 81–93.

Teller, J. T., Leverington, D. W. & Mann, J. D. 2002. Freshwater outbursts to the oceans from glacial Lake Agassiz and their role in climate change during the last deglaciation. *Quaternary Science Reviews* **21,** 879–887.

ter Braak, C.J.F., Juggins, S., 1993. Weighted averaging partial least squared regression (WA-PLS): an improved method for reconstructing environmental variables from species assemblages. *Hydrobiologia* **269**, 270, 485–502.

Thomas, E.R., Wolff, E.W., Mulvaney, R., Steffensen, J.P., Johnsen, S.J., Arrowsmith, C., White, J.W.C., Vaughn, B., Popp, T. 2007. The 8.2 ka event from Greenland ice cores. *Quaternary Science Reviews* **26**, 1-2, 70-81.

Törnqvist, T.E., Hijma, M.P. 2012. Links between early Holocene ice-sheet decay, sea-level rise and abrupt climate change, *Nature Geoscience* **5**, 601-606. DOI: 10.1038/NGEO1536.

Troels-Smith, J. 1955. Karakterisering af lose jordarter.Characterisation of unconsolidated sediments, *Geological Survey of Denmark*, **4**, 3, 1-73.

Vos, Peter C., de Wolf, H., 1993. Diatoms as a tool for reconstructing sedimentary environments in coastal wetlands; methodological aspects. In: Twelfth International Diatom Symposium. Springer, Netherlands, 285-296.

Ward, S. L., 2014. A new proxy for constraining palaeotidal model simulation of the Northwest European Shelf Seas. Doctoral thesis, Bangor University.

Wells, J. M. 1997. *Flandrian relative sea level changes in the Cree estuary region, southwest Scotland.* Doctoral thesis. Coventry University.

Wiersma AP, Renssen H. 2006. Model–data comparison for the 8.2 ka BP event: confirmation of a forcing mechanism by catastrophic drainage of Laurentide lakes. *Quaternary Science Reviews* **25**, 63–88.

Wiersma, A.P., Jongma, J.I. 2010. A role for icebergs in the 8.2 ka climate event, *Climate Dynamics* **35**, 535-549.

Wiersma, A.P., Roche, D.M., and Renssen, H. 2011. Fingerprinting the 8.2 ka climate response in a coupled climate model, *Journal Quaternary Science* 26, 1, 118-127.

Wilson, G.P., and Lamb, A.L. 2011. An assessment of the utility of regional diatom-based transfer functions. *Journal Quaternary Science* **27**, 4, 360-370. DOI: 10.1002/jqs.1553.

Zecchin, M., Tosi, L., Caffau, M., Baradello, L., Donnici, S. 2014. Sequence stratigraphic significance of tidal channel systems in shallow lagoon (Venice, Italy). *The Holocene* **24**, 6. doi:10.1177/0959683614526903.

Zong, Y. and Tooley, M.J. 1996. Holocene sea-level changes and crustal movements in Morecambe Bay, northwest England. *Journal of Quaternary Science* 11(1), 43-58.

Zong, Y., Horton, B.P. 1999. Diatom-based tidal-level transfer functions as an aid in reconstructing Quaternary history of sea-level movements in the UK. *Journal Quaternary Science* **14**, 2, 153-167.

Figure

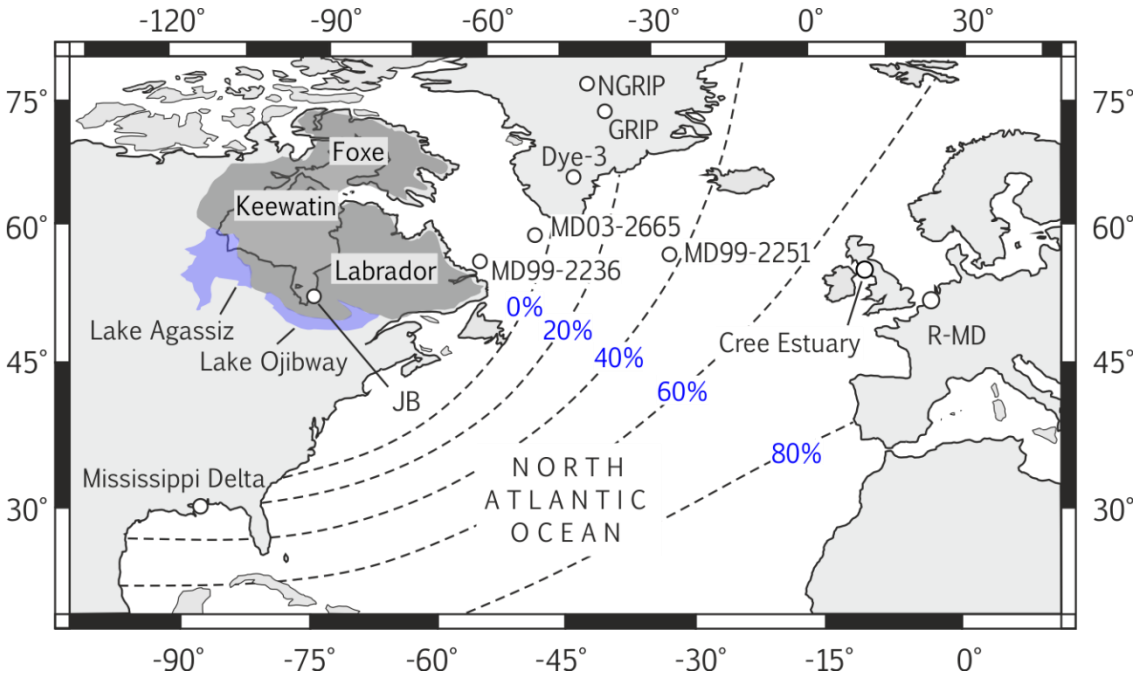

Figure 1. Map of circum-North Atlantic with key locations mentioned in text. Blue and dark grey shading indicates the approximate extent of Laurentide Ice Sheet and proglacial lakes Agassiz and Ojibway at ~8900 cal yr BP (after Dyke, 2004). Dashed lines denote the spatial variability of RSL rise associated with a LAO source of meltwater release from GIA modelling (after Kendall et al., 2008). JB = James Bay. R-MD = Rhine-Meuse Delta.

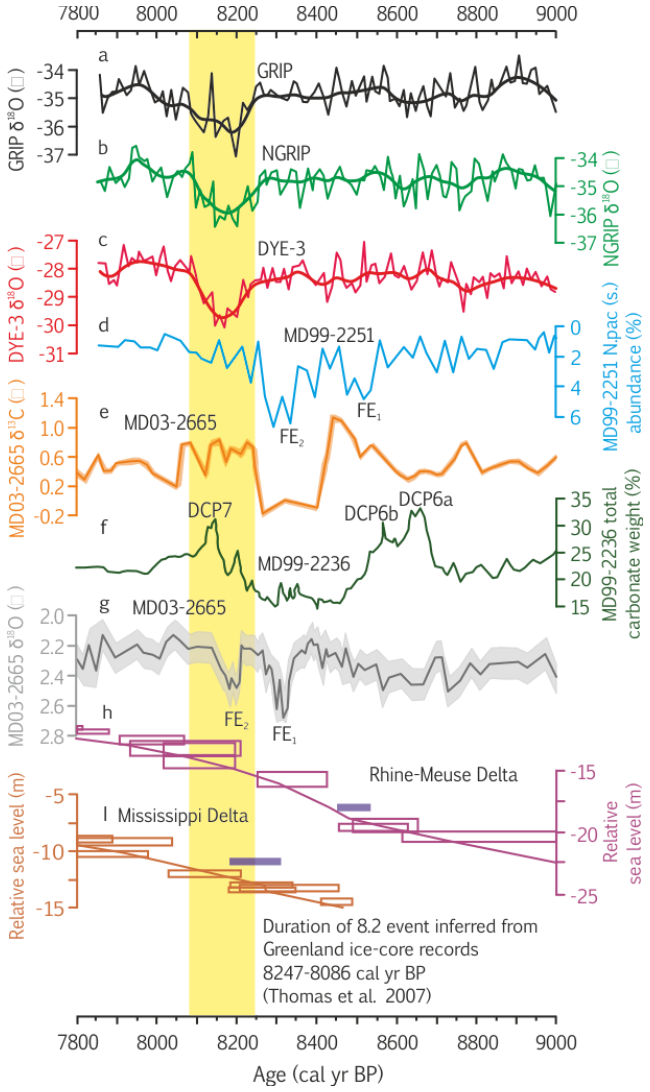

Figure 2. Records of early Holocene climate, oceanographic and sea-level change in the North Atlantic. Ages are calibrated with respect to AD 1950. **a**, GRIP $\delta^{18}O$ with a 50 yr moving Gaussian smoothing. **b**, NGRIP $\delta^{18}O$ with a 50 yr Gaussian smoothing **c,** Dye-3 $\delta^{18}O$ with a 50 yr Gaussian smoothing. **d**, *Neogloboquadrina pachyderma* (s.) abundance in North Atlantic deep sea sediments (Ellison et al., 2006). **e,** *Neogloboquadrina pachyderma* s. $\delta^{13}C$ in Labrador Sea sea-floor sediments (Kleiven et al., 2008), on revised chronology (this study). FE_1 = Freshening Event 1; FE_2 = Freshening Event 2 (see text). **f,** Percentage detrital carbonate by weight in Cartwright Saddle sea-floor sediments (Jennings et al., 2015). DCP events correspond to 'detrital carbonate peaks'. **g,** *Neogloboquadrina pachyderma* s. $\delta^{18}O$ record in Labrador Sea sea-floor sediments (Kleiven et al., 2008), on its revised chronology (this study). FE_1 = Freshening Event 1; FE_2 = Freshening Event 2 (see text). **h,** Relative sea-level record from the Rhine-Meuse delta defined as 2σ age and vertical uncertainty error boxes (Hijma and Cohen, 2010). Blue bar denotes 2σ age range of the start of the RSL jump (Table 2). **i**, Relative sea-level record from the Mississippi Delta defined as 2σ age and vertical uncertainty error boxes (Li et al., 2011). Blue bar denotes 2σ age range that encompasses the RSL jump in its entirety (Table 2). Yellow bar indicates duration of the 8.2 event as inferred from a 'stack' of Greenland ice core records (Thomas et al., 2007).

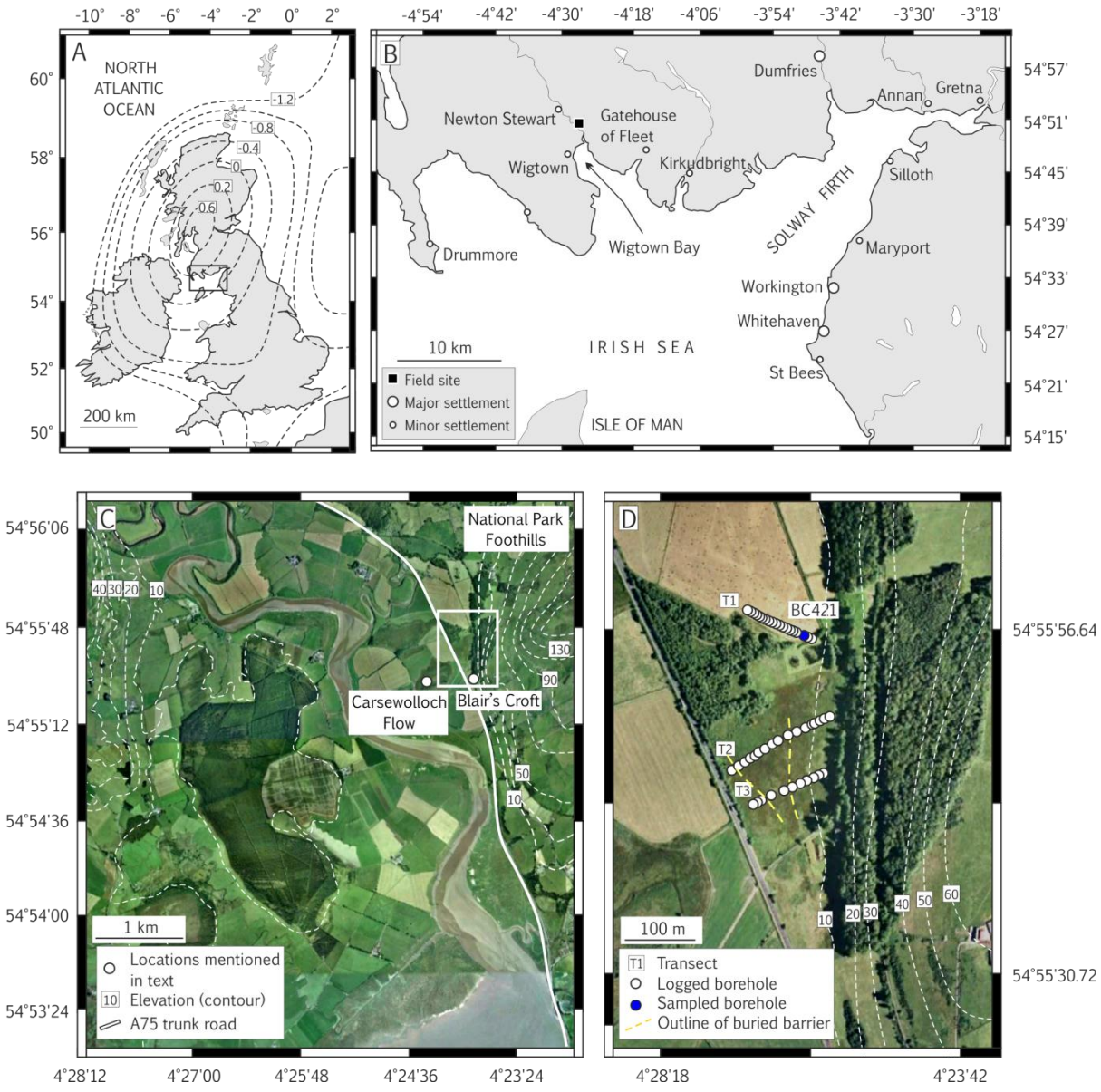

Fig. 3. Location maps of field site in southwest Scotland. A) Map of UK and Ireland overlain with the contour lines of the present-day vertical land motions determined by the glacio-isostatic adjustment model of Bradley et al. (2011), denoting uplift rates in mm yr^{-1}. B) Setting of Solway Firth in the Irish Sea and the location of Wigtown Bay and the Cree Estuary. C) Google Earth image of the Cree Lowlands and locations mentioned in text. D) Google Earth overview of Blair's Croft field-site and borehole locations.

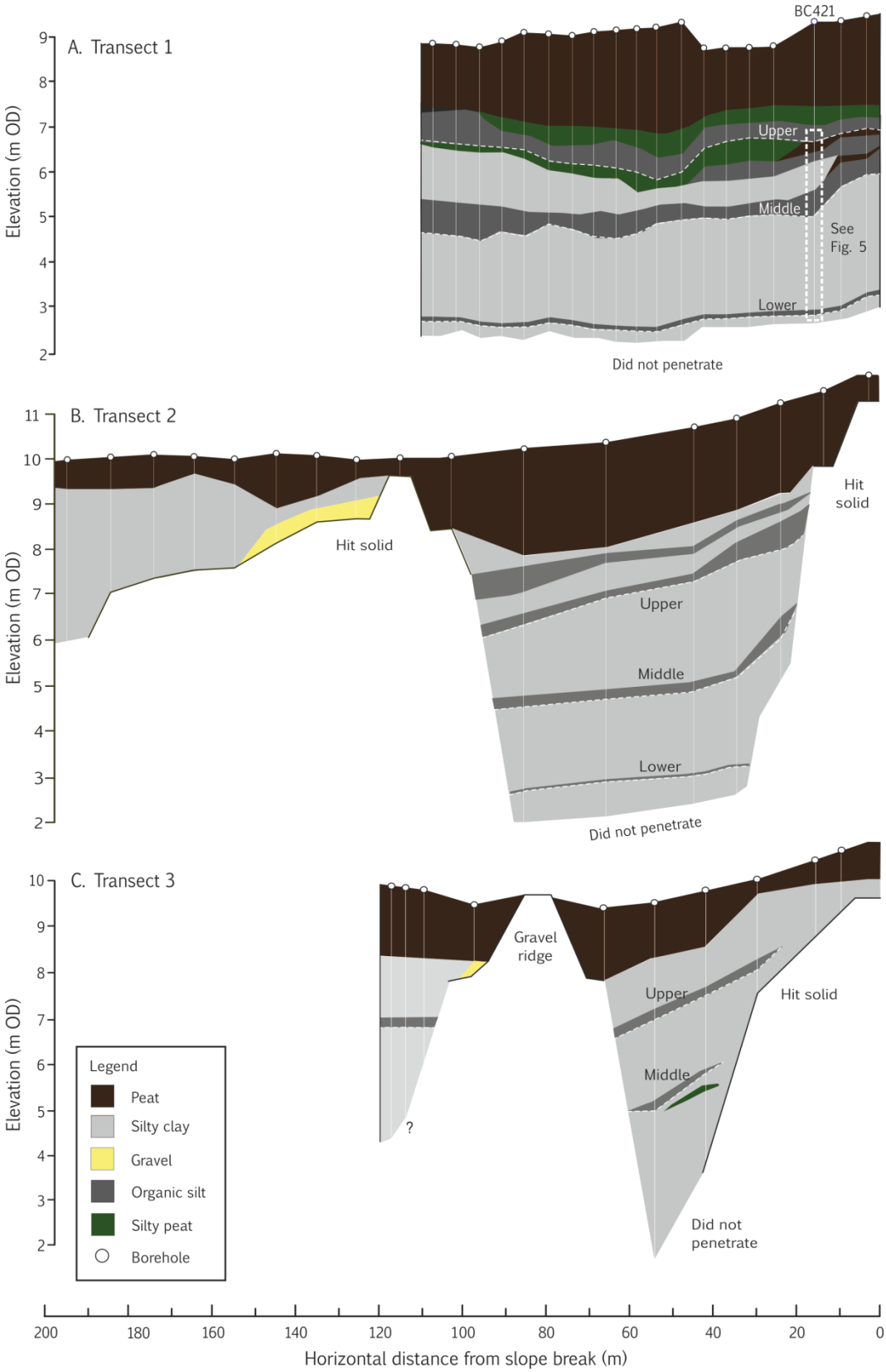

Figure 4. Lithostratigraphy of Blair's Croft recorded along A) Transect 1, B) Transect 2 and C) Transect 3. The reader is referred to Figures 3 and 5 for core locations and ^{14}C dating of core BC421, respectively. To aid in correlations, organic beds 'lower', 'middle' and 'upper' are illustrated, but we note that our focus is on the sedimentary sequence illustrated by the stipple white outline in Transect 1 which here encompasses the lower and middle beds and their overlying minerogenic deposits.

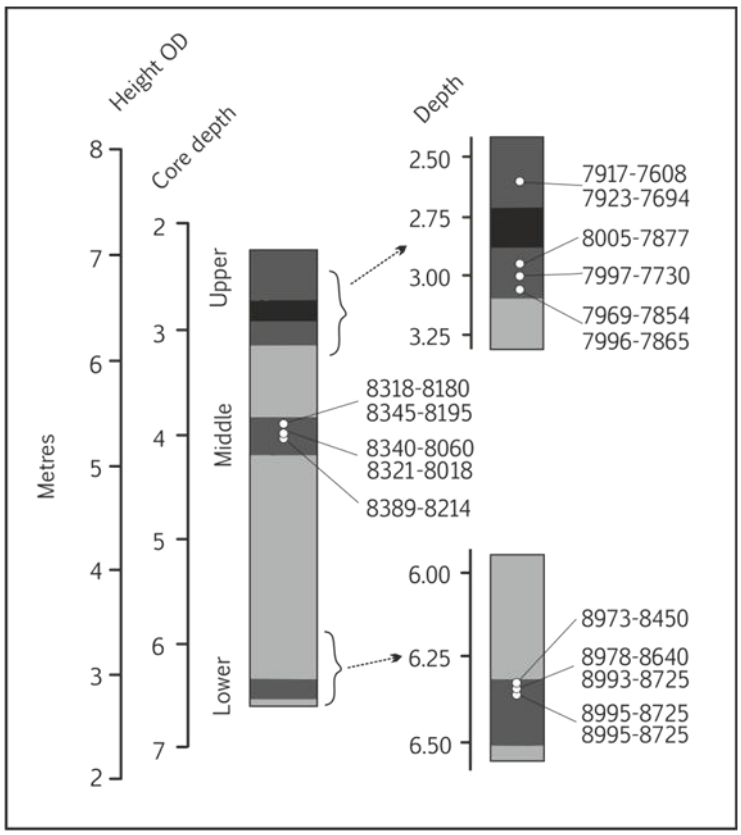

Figure 5. Radiocarbon dating of core BC421. Ages are reported as 2σ calibrated ranges (IntCal 13; Reimer et al., 2013).

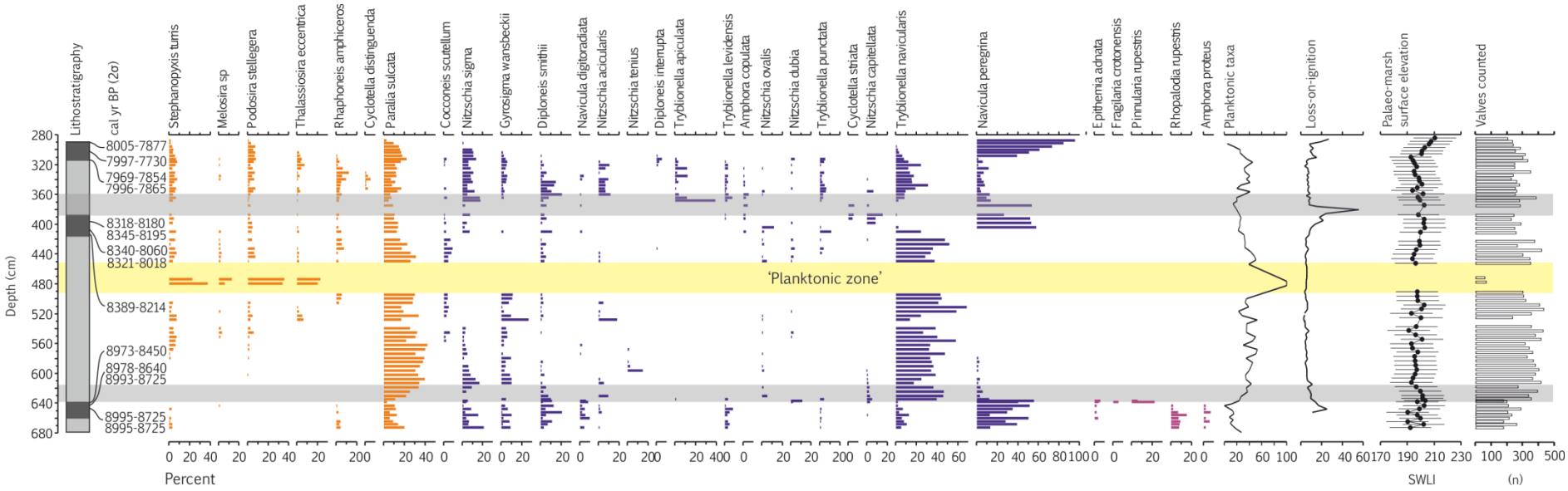

Figure 6. Diatom biostratigraphy, chronostratigraphy and LOI of core BC421. Diatom contributions represent >5%. Palaeomarsh surface elevation (in SWLI units) is reconstructed using the component-two model (WA-PLS) of the 'screened' training set. For a more detailed view of sample depths of ^{14}C ages, refer to Figure 5 and Table 1. Marine taxa (planktonic forms) are indicated in orange, brackish-indifferent taxa in blue and freshwater-brackish taxa in purple. Yellow shading indicates the 'planktonic zone'. Gray shading indicates abrupt reductions in SWLI that are accompanied by stratigraphic evidence of marsh drowning (see discussion).

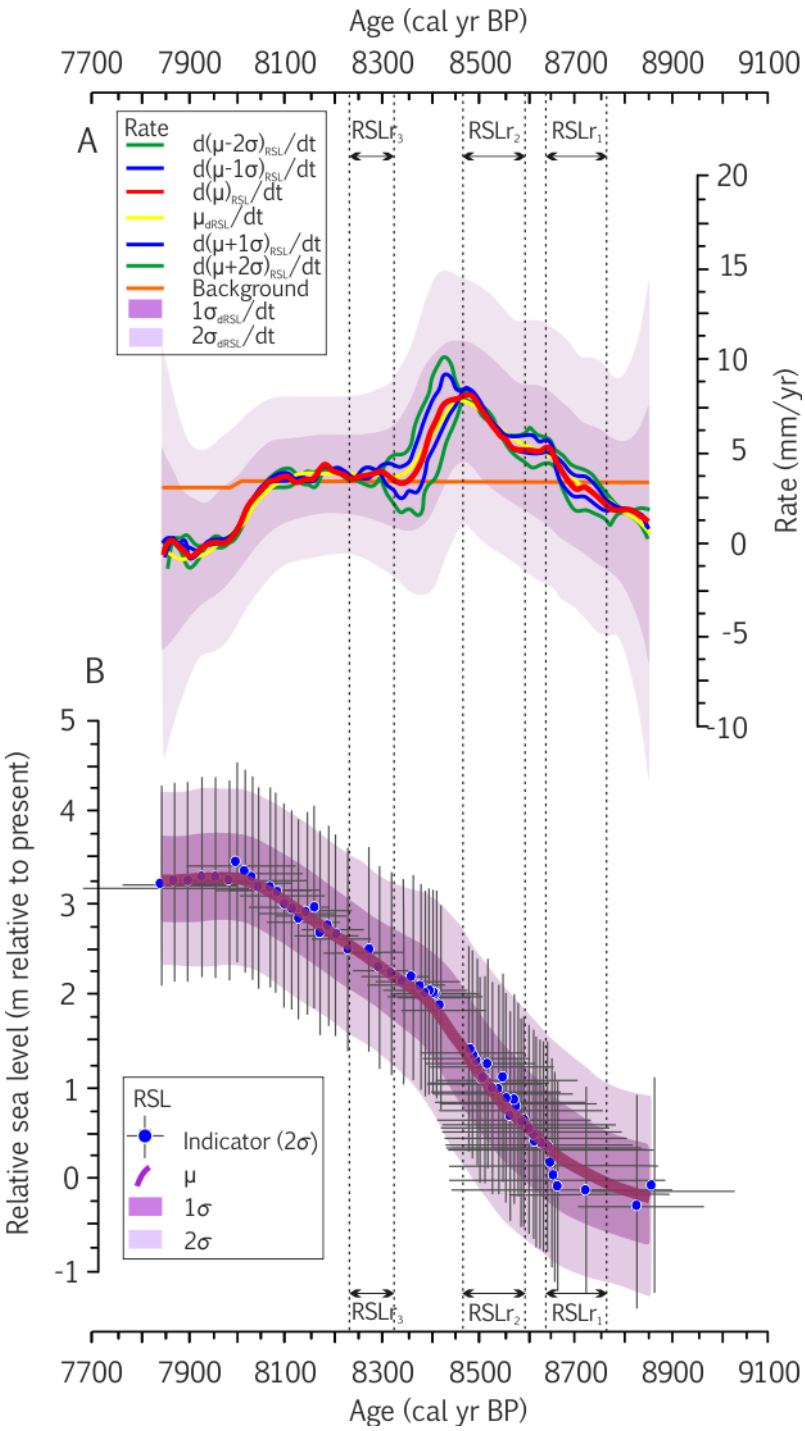

Figure 9. Relative sea-level change in the Cree Estuary for the period 8800 -7700 cal yr BP. **a.** Rates of relative sea-level change in **a**. are inferred from the relative sea-level reconstruction in **b.** The orange line depicts site-specific rates of millennial-scale RSL change as depicted by the Bradley et al. (2011) GIA model. RSL jumps (dashed lines; $RSLr_1$, $RSLr_2$, $RSLr_3$) are determined where rates of rise exceed the background trend in three differentiated RSL curves ($d\mu_{RSL}/dt$, $d(\mu-\sigma)_{RSL}/dt$, $d(\mu+\sigma)_{RSL}/dt$).

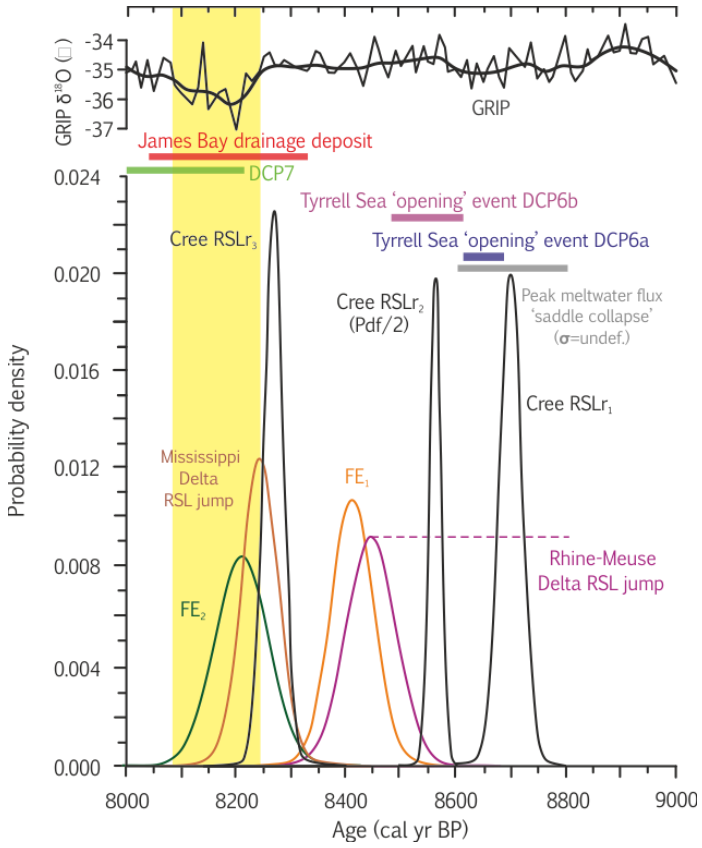

Figure 8. Timing and sequence of climate, ocean and sea-level events in the North Atlantic between 9000 and 8000 cal yr BP. Timing of events are expressed as age probability density functions (pdfs) (3σ) and horizontal bars (2σ probability ranges). Probability density functions of $RSLr_1$, $RSLr_2$ and $RSLr_3$ (black curves) in the Cree estuary from this study are plotted alongside DCP6a (blue bar) and DCP6b (purple bar) from Jennings et al. (2015), the James Bay drainage deposit (red bar; Roy et al., 2005), the onset of sudden sea-level rise in the Rhine-Meuse Delta (purple curve; Hijma and Cohen, 2010) and Mississippi Delta (brown curve; Li et al., 2012) and the two North Atlantic surface cooling and freshening events (FE_1; orange curve, FE_2 light blue curve) inferred from revised chronology of Kleiven et al. (2008). Peak meltwater discharge (modelled) associated with separation of the Keewatin and Labrador ice-dome 'saddle' (Gregoire et al., 2012) is shown as a grey bar, but note has no strict statistical definition. Yellow shading depicts the full duration of the 8.2 event as determined from Greenland ice-core records by Thomas et al. (2007).

Table 1. Radiocarbon dates from BC421. Samples B1(a) and B1(b) (dark gray) are excluded from the age model because they are taken from the base of the 'upper' organic bed and are too young to be associated with the 8.2 kyr BP event, but provide a maximum age of barrier activity at its present position. Sample B is not included because of a minor age reversal with preceding samples (light grey). AMS = accelerator mass spectrometry. *Calibrated with the IntCal13 calibration curve (Reimer et al. 2013) in OxCal 4.2 (Bronk Ramsey, 2008). Modelled weighted means of duplicate ages are highlighted bold.

Sample Code	Identifier	Depth (cm)	Height (m OD)	Dating method	Material dated	Reported ^{14}C age (±1σ lab error)	Calibrated* range (2σ)
SUERC-44407	B1(b)	259.5	6.90	Duplicate AMS	*Phragmites australis*	6890 ± 64	7917-7608
SUERC-44406	B1(a)	259.5	6.90	Duplicate AMS	*Phragmites australis*	6963 ± 36	7923-7694
SUERC-44405	B	294.5	6.55	Single AMS	*Phragmites australis*	7127 ± 26	8005-7877
SUERC-44400	C	300.5	6.49	Single AMS	*Phragmites australis*	7049 ± 65	7997-7730
SUERC-42712	D(b)	307	6.42	Duplicate AMS	*Phragmites australis*	7088 ± 26	7969-7854
SUERC-44399	D(a)	307	6.42	Duplicate AMS	*Phragmites australis*	7107 ± 26	7996-7865 **(7968-7871)**
SUERC-44371	Q(b)	389	5.60	Duplicate AMS	*Alnus*	7409 ± 26	8318-8180
SUERC-42711	Q(a)	389	5.60	Duplicate AMS	*Alnus*	7452 ± 25	8345-8195 **(8315-8188)**
SUERC-44398	R(b)	395.5	5.54	Duplicate AMS	*Phragmites australis*	7344 ± 65	8321-8018
SUERC-44397	R(a)	395.5	5.54	Duplicate AMS	*Phragmites australis*	7392 ± 39	8340-8060 **(8339-8201)**
SUERC-44386	T	402	5.47	Single AMS	*Phragmites australis*	7507 ± 25	8389-8214
SUERC-44387	U	631	3.18	Single AMS	*Phragmites australis*	7831 ± 65	8973-8450
SUERC-42709	V(b)	632	3.17	Duplicate AMS	*Alnus*	7936 ± 27	8978-8640
SUERC-44385	V(a)	632	3.17	Duplicate AMS	*Alnus*	7977 ± 26	8993-8725 **(8936-8650)**
SUERC-44369	W(b)	632	3.17	Duplicate AMS	*Alnus*	7980 ± 27	8995-8725

SUERC-42708	W(a)	633	3.16	Duplicate AMS	*Alnus*	7982 ± 27	8995-8725 **(8960-8660)**

	Position in stratigraphy / record	**Minimum age (cal yr BP)**	**Maximum age (cal yr BP)**	**Minimum age (yrs BP) from start of 8.2 event**	**Maximum age (yrs BP) from start of 8.2 event**	**Reference**
8.2 event	All	8086	8247	0	0	Thomas et al. (2007)
Cree Estuary $RSLr_3$	Start	8218	8323	-29	237	This study
FE_2	Start	8114	8308	-133	222	Kleiven et al. (2008); this study
Mississippi Delta	All	8180	8310	-67	224	Li et al. (2011)
James Bay drainage deposit	All	8032	8323	-215	237	Roy et al. (2011)
FE_1	Start	8338	8492	91	406	Kleiven et al. (2008); this study
Cree Estuary $RSLr_2$	All	8465	8595	288	509	This study
Rhine-Meuse Delta	Start	8455	8587	208	501	Hijma and Cohen (2010)
Cree Estuary $RSLr_1$	Start	8640	8760	393	674	This study
DCP6b	Start	8489	8609	242	523	Jennings et al. (2015)
Keewatin and Labrador saddle collapse	Peak	8600	8800	353	714	Gregoire et al. (2012)
DCP6a	Start	8609	8694	362	608	Jennings et al. (2015)

Table 2. Timing of abrupt events within the critical time interval. Ages presented are 2σ calibrated ranges with respect to BP (AD 1950), with the exception of the Cree RSL jumps (3 sigma of the differentiated record) and the Thomas et al. (2007) estimate of the timing of the 8.2 event (full 3 sigma uncertainty range).

Table 3. Magnitudes of abrupt sea-level change within the critical time interval. Local magnitude (Local) and Fingerprint-corrected value (Global) assumes a LIS source of freshwater release with fingerprint values of 20% for the Mississippi Delta and 70% for the Cree Estuary and Rhine-Meuse Delta, respectively (after the geophysical model predictions of Kendall et al. (2008).

	Differentiated RSL curve reconstruction						RSL rate reconstruction				
	$d(\mu-2\sigma)_{RSL}/dt$	$d(\mu-\sigma)_{RSL}/dt$	$d\mu_{RSL}/dt$	$d(\mu+\sigma)_{RSL}/dt$	$d(\mu+2\sigma)_{RSL}/dt$		$(\mu-2\sigma)_{dRSL/dt}$	$(\mu-\sigma)_{dRSL/dt}$	$\mu_{dRSL/dt}$	$(\mu+\sigma)_{dRSL/dt}$	$(\mu+2\sigma)_{dRSL/dt}$
$RSLR_3$											
Local	0.37	0.39	0.40	0.41	0.43		-0.10	0.15	0.40	0.65	0.90
Global	0.54	0.55	0.57	0.59	0.61		-0.15	0.21	0.57	0.93	1.29
$RSLR_2$											
Local	0.67	0.69	0.70	0.72	0.73		-0.05	0.27	0.66	1.05	1.44
Global	0.96	0.98	1.00	1.02	1.04		-0.07	0.39	0.95	1.50	2.06
$RSLR_1$											
Local	0.24	0.30	0.35	0.40	0.45		-0.42	-0.03	0.36	0.75	1.15
Global	0.35	0.42	0.50	0.57	0.65		-0.60	-0.04	0.52	1.08	1.64
Sum total of $RSLr_1$ and $RSLr_2$:											
Local	1.34	1.40	1.45	1.50	1.56		-0.58	0.39	1.42	2.46	3.49
Global	1.92	2.00	2.07	2.15	2.23		-0.82	0.56	2.03	3.51	4.99